Distinct sources and behavioral correlates of macaque motor cortical low and high beta

Simon Nougaret, Laura López-Galdo, Emile Caytan, Julien Poitreau, Frédéric Barthélemy, Bjørg Elisabeth Kilavik

Distinct sources and behavioral correlates of macaque motor cortical low and high beta

Simon Nougaret[1,*], Laura López-Galdo[1], Emile Caytan[1,2], Julien Poitreau[1,3], Frederic V Barthelemy[4,1], Bjørg Elisabeth Kilavik[1,*]

[1] Institut de Neurosciences de la Timone (INT), UMR 7289, CNRS, Aix-Marseille Université, Marseille 13005, France

[2] Current address: University of Crete, Faculty of Medicine & Foundation for Research and Technology Hellas, Institute of Applied and Computational Mathematics, Heraklion 70013, Greece

[3] Current address : Laboratoire de Neurosciences Cognitives (LNC), UMR 7291, CNRS, Aix-Marseille Université, Marseille, France

[4] Institute of Neuroscience and Medicine (INM-6) and JARA Institute Brain Structure-Function Relationships (INM-10), Jülich Research Centre, Jülich, Germany

*Corresponding authors: Simon.Nougaret@univ-amu.fr, Bjorg.Kilavik@univ-amu.fr

HIGHLIGHTS:

- The low beta rhythm is dominant in M1 and the high beta rhythm in PMd
- The beta rhythms correlate with task-instructed and uninstructed behavior
- Low beta reflects movement preparation and spontaneous postural dynamics
- High beta reflects temporal task prediction and dynamical visuospatial attention

BRIEF SUMMARY: Nougaret et al. find that low and high beta rhythms co-reside in motor cortex. Low beta dominates in M1 and reflects movement preparation but also uninstructed postural changes. High beta dominates in PMd and reflects temporal task prediction but also fluctuations in focal overt attention dedicated to the behavioral task.

Keywords: macaque, local field potentials, motor cortex, beta rhythms, spontaneous movements, postural control, movement preparation, attention, anticipation

SUMMARY

Low and high beta frequency rhythms were observed in motor cortex, but their respective sources and behavioral correlates remain unknown. We studied local field potentials during pre-cued reaching behavior in macaques. They contained a low beta band (<20Hz) dominant in primary motor cortex and a high beta band (>20Hz) dominant in dorsal premotor cortex. Low beta correlated positively with behavioral reaction time, from visual cue onset, and negatively with uninstructed hand postural micro-movements throughout the trial. High beta reflected temporal task prediction, with selective modulations before and during cues that were enhanced in moments of increased focal attention, when the gaze was on the work area. This double-dissociation in cortical sources and behavioral correlates of motor cortical low and high beta, with respect to both task-instructed and spontaneous behavior, reconciles the largely disparate roles proposed for the beta rhythm, by suggesting band-specific roles in both movement control and spatio-temporal attention.

INTRODUCTION

A link between the beta rhythm in human sensorimotor cortex and voluntary movements was established almost 75 years ago (Jasper and Penfield 1949). Yet, the functional role of sensorimotor beta remains elusive. Beta was associated with many aspects of motor behavior, ranging from motor cortical idling or postural maintenance (e.g. Salmelin et al. 1995; Conway et al. 1995; Baker et al. 1999; Brown 2000; Engel and Fries 2010; van Ede et al. 2010, 2011; Jenkinson and Brown 2011; Khanna and Carmena 2017; Peles et al. 2020) to sensorimotor integration or temporal predictions (e.g. Murthy and Fetz 1992, 1996; Sanes and Donoghue 1993; Rubino et al. 2006; Androulidakis et al. 2006; Lalo et al. 2007; Saleh et al. 2010; Fujioka et al. 2012; Kilavik et al. 2014; Wiener et al. 2018; Sun et al. 2021). As beta rhythms were observed in many cortical and sub-cortical regions and in many different behavioral contexts, they might serve multiple roles (Kilavik et al. 2013; Spitzer and Haegens 2017; Schmidt et al. 2019; Barone and Rossiter 2021).

Most studies have treated the broad beta frequency range (~13-35Hz) as one common motor cortical rhythm, possibly rendering the association of specific beta rhythm modulations to specific components of sensorimotor behavior difficult. A few studies divided this broad band into low beta (below 20Hz) and high beta (above 20Hz). In a published dataset (Kilavik et al. 2012; Confais et al. 2020) we observed concurrent and distinct low and high beta bands during visuomotor behavior in macaque motor cortical local field potentials (LFP). However, the low and high bands modulated similarly in power and peak frequency in that behavioral task. Also Stoll et al. (2015) observed two distinct low and high beta bands in macaque frontal cortical electrocorticography (ECoG), in a trial-and-error task, comprising search and repetition phases. They found only the high band to be systematically sensitive to attentional effort and cognitive control. Chandrasekaran et al. (2019) correlated behavioral reaction time (RT) with dorsal premotor cortex (PMd) beta power, in a visual RT-task. In the pre-stimulus period, they found positive correlations for frequencies below 20Hz and negative correlations for frequencies above 20Hz. However, their data only contained a single beta band peaking at 25Hz, which shifted slightly towards higher peak frequency for shorter RT. In

comparison, Zhang et al. (2008) found positive correlations with RT for sensorimotor pre-stimulus alpha/beta power across a broad frequency range of 8-33Hz in a visual RT task.

These studies remain far from conclusive in determining potentially distinct correlations between behavior and motor cortical low and high beta bands. We therefore designed a new visuomotor behavioral task to maximize at the same time spatio-temporal attention and the required motor control, with the aim to disentangle which of the different task variables, and task-instructed and uninstructed (spontaneous) behavioral factors (Musall et al. 2019; Tremblay et al. 2022 bioRxiv) affect the two beta bands. We hypothesized that low beta might be related to dynamic postural control and movement preparation. This band was shown to be more affected in human Parkinson's disease patients than high beta (Kühn et al. 2009; Neumann et al. 2016), and was also more attenuated by deep-brain stimulation in the subthalamic nucleus (Lopez-Azcarate et al. 2010) and by levodopa administration (Priori et al. 2004), that both improve motor performance in the patients. In contrast, motor cortical high beta might be more closely associated with attentional, decisional or working memory processes (Stoll et al. 2015; Lundqvist et al. 2016; Haegens et al. 2017), and located anterior to low beta (Vezoli et al. 2021). Consistent with these predictions, in two macaques we found low beta to be dominant in primary motor cortex (M1) and correlate positively with behavioral RT. Low beta also correlated negatively with spontaneous hand postural micro-movements that were frequent during the maintenance of stable central hold during delays. High beta, on the other hand, was dominant in PMd, and was unrelated to RT and hand micro-movements. It modulated selectively in anticipation of and during the processing of visual cues. This modulation was enhanced by focal overt attention, when the animal oriented the gaze towards the work area.

RESULTS

We studied LFP low and high beta band rhythms recorded in the motor cortex (M1 and PMd) of two macaque monkeys engaged in a complex visuomotor reaching task. We determined the motor cortical regions in which each band dominated, and we quantified their relationship to task conditions and performance, and to spontaneous hand and eye movements.

Behavioral task performance and uninstructed hand and eye movements

Two macaque monkeys performed a rule-based and predictive visual cue selection task, requiring arm reaching responses after a GO signal, in one of 4 (diagonal) directions from a common center position. The monkeys did many errors related to selecting the wrong visual cue or by not maintaining central hand position through the delays. They also performed spontaneous hand and eye movements that were aligned to task events.

We analyzed the behavior in 59 sessions obtained in 53 recording days in monkey T and 39 sessions in 34 days in monkey M, from which electrophysiological data was also analyzed. The visuomotor task was complex, requiring the animal to select the valid spatial cue (SC; one out of three sequentially presented SCs; the other two were distractors) that matched in color with a preceding color selection (SEL) cue (Fig. 1B). The animal then had to prepare a center-out arm reaching movement to the memorized matching SC position, to be executed after a GO signal. Throughout the sequence of presentation of the different visual cues, the animal had to maintain central hand position with the manipulandum, but was free to explore the visual scene with the eyes.

In trials initiated by the monkey, the maintenance of central hand position on the small central fixation spot was often lost before the GO signal (41.9 % of initiated trials for monkey T and 37.8 % for monkey M). A majority of breaks of hand fixation happened early in the trial, before SEL cue onset (24.8% and 15.9% of the initiated trials in monkey T and M, respectively). The remaining hand fixation breaks were distributed across the remaining delays between SEL and GO (only 3-6% of the initiated trials in each delay). This abundance of aborted trials due to hand fixation breaks

demonstrate the difficulty of initial stabilization and maintenance of the hand manipulandum within the 0.6cm diameter fixation zone in the manual space.

Several types of errors were also made in trials not aborted before the GO signal was presented (*GO trials*). Of these, errors caused by too long reaction or movement times were not very frequent (1.3% and 7.4 % of all GO trials in monkey T, 4.4% and 2.2% in monkey M, respectively). Directional errors due to selecting a peripheral position not cued by any of the two distractors were also rare (1.7% of all GO trials in money T, 3.0 % in monkey M).

Directional errors towards a distractor direction (*distractor errors*) were much more frequent, accounting for 17.4% of all GO trials in monkey T and 22.3% in monkey M. These distractor errors occurred less frequently for the pink color condition (SC3 valid; Fig. 1B) in both monkeys ($p<0.01$ for both monkeys; multiple comparison chi-squared test using Matlab function crosstab; Suppl. Table 1). The distractor errors furthermore varied slightly across the four movement directions for both animals, with somewhat less errors for movements towards the body (i.e. lower visual field) than away from the body (i.e. upper visual field) ($chi2=28.6$, $p<0.01$ for monkey T, $chi2=8.5$, $p=0.036$ for monkey M; suppl. Table 1).

The RT (time between GO and reach movement onset) was calculated offline from the hand trajectories (see Methods). We analyzed variability in RT across the recorded sessions, color conditions and movement directions for each monkey, using 3-way ANOVAs. All three factors significantly affected RT in a similar manner in the two animals ($p<0.01$; Suppl. Table 1). First, there was a significant main effect of session, but with no systematic trend with increasing or decreasing RT from early to late sessions. Furthermore, RT varied significantly across the three conditions, with shorter RT in the pink color condition. Finally, RT varied slightly across the four movement directions, with slightly shorter RT for movements towards than away from the body. Averaged RT was only 6-23ms longer in monkey M than in monkey T.

Both animals made spontaneous (uninstructed) movements during the behavioral trial (see Musall et al. 2019; Tremblay et al. 2022 bioRxiv). This included hand micro-movements during the

maintenance of central position, with the hand position remaining within the central fixation spot (Fig. 1C), and eye gaze shifts (saccades) to and from the work area (computer monitor), and to explore the elements of the visual scene within the work area (Fig. 1D-F). Although uninstructed, these hand and eye movements were remarkably similar in the two animals, and aligned to task events.

The hand micro-movements during central position maintenance were quantified by velocity. The average hand velocity decreased as the hand stabilized inside the central fixation spot at the start of the trial, and was minimal before the onset of the valid SC. After the presentation of the valid SC, hand velocity increased, and therefore differed significantly in the three conditions (Fig. 1C and Suppl. Fig. 1A-B and D). These micro-movements did not reflect a drift of the hand position in the (diagonal) direction of the upcoming center-out reaching movement (Suppl. Fig. 1C), unlike the spatial attention effects described for eye fixational microsaccades (Hafed and Clark 2002). Instead, the hand prevalently drifted along one of the two main axes defined by the 2D manipulandum, having lower frictional resistance. Control electromyographic (EMG) recordings from the deltoid muscle revealed increased muscular tone during the preparatory period following the valid SC onset (Suppl. Fig. 1E). This increase tone was similar for preparation of movements towards and away from the body, thus also not displaying any directionality, in contrast to the strong selectivity of this muscle during the center-out reach execution. Thus, the hand micro-movements during movement preparation were at least partly caused by increased muscle tone of arm muscles involved in the following reaching movement.

The monkeys frequently made saccadic eye movements to explore the items of the visual scene, or to shift the gaze towards or away from the work area (Fig. 1D-F). On average, the probability to perform a saccade (in the direction of the cue) increased transiently after each visual cue, in a condition-selective manner, with more frequent gaze shifts towards the location of the valid SC than the invalid SC (distractor; Fig. 1E-F). The gaze was often directed out of the work area of the visual scene, and more so for monkey M than monkey T, but in both animals less frequently around the

time of the valid SC and as the GO signal approached. Each trial lasted longer than 6 seconds, and the visual scene had salient cues presented for 300ms each, so that their color and location could most likely also be detected with peripheral vision (*covert* attention), triggering a saccade towards the cue, not requiring constant *focal* or *overt* attention with the gaze constantly directed within the visual scene. Finally, both monkeys restricted eyeblinks to the delays, and more so after having fixated the valid SC, thus under tight temporal attentional control, as also shown in humans engaged in demanding working memory tasks (Ortega et al. 2022).

To summarize, the behavioral task performance was very similar for the two animals. Both animals had faster RT and less distractor errors for the pink color condition and for movement directions towards the body. Also spontaneous hand micro-movements and eye gaze shifts were aligned to task events in a remarkably similar manner in both animals.

Concurrent low beta in M1 and high beta in PMd

Both monkeys had two bands in the beta frequency range, one peaking below and the other above 20Hz in motor cortex. Low beta (<20Hz) was dominant in M1 and high beta (>20Hz) was dominant in PMd.

LFP activity from 110 individual sites in monkey T and 60 sites in monkey M, across M1 and PMd was analyzed. Spectrograms for an example session with three simultaneously recorded LFP sites (Fig. 2A-C) showed a high beta band (> 20Hz) predominant in the most anterior site (PMd; site 1), and a low beta band (<20Hz) predominant in the most posterior site (M1; site 3). Both bands were distinguishable in the intermediate site (site 2). Even if the trial-averaged spectrograms showed increased beta band power across long periods of the task, single-trial LFPs showed bursts of high beta in PMd (Fig. 2D) and low beta in M1 (Fig. 2F) of variable durations and timing across trials, as already described (e.g. Murthy and Fetz 1996; Donoghue et al. 1998; Feingold et al. 2015; Confais et al. 2020).

193 Average spectrograms across all trials and LFP sites for each monkey (Fig. 2E) confirmed the
194 presence of a low and a high beta band in both animals, with the low band peaking at 15-16Hz, and
195 the high band at 25-26Hz (Fig. 3A). We computed a *beta band dominance index* (see Methods) in the
196 pre-SC1 epoch, as both bands were present in this epoch in the single site examples and in the
197 average spectrograms for both monkeys (Fig. 3B). A majority of sites had a dominant low beta band
198 (positive indices), but in both animals a substantial fraction of sites had a significant high beta band
199 dominance. Overlaying the beta band dominance index on the cortical surface reconstruction within
200 the recording chamber, a gradient across the cortical surface was found in both animals, with the
201 high band predominant in the most anterior recording sites (PMd), and the low band predominant in
202 the posterior sites (M1) and in the intermediate sites (Fig. 3C). There was a significant (negative)
203 correlation between band dominance index and antero-posterior (or PMd-M1) gradient within the
204 recording chamber for both animals ($p<0.01$; Spearman's rank order correlation). To confirm local
205 origin of these LFP beta rhythms, we analyzed phase-locking of the simultaneously recorded neurons
206 to the locally dominant beta band, for neurons and LFPs recorded on the same linear array. For the
207 low beta band dominant sites, 11.2% of neurons (25/311 neurons in monkey T and 37/241 in monkey
208 M) were significantly phase-locked to low beta phase. For the high beta band dominant sites, 51.1%
209 of neurons (13/24 neurons in monkey T and 34/68 in monkey M) were significantly phase-locked to
210 high beta phase. The average spectrograms, plotted separately according to beta band dominance,
211 are remarkably similar in the two animals, with very distinct modulations for each band (Fig. 3D),
212 which we further detail below.

213 In summary, low and high beta peak frequencies (Fig. 3A), the beta band dominance across the
214 cortical surface (Fig. 3C) and task-related modulations of each band (Fig. 3D) were similar in the two
215 animals. Also task performance (Suppl. Table 1) and spontaneous hand and eye movements (Fig. 1C-
216 F) were similar in the two monkeys. From hereon we therefore collapsed the data for the two
217 animals. In particular, we combined all individual trials from all LFP sites with the same beta band
218 dominance, such that each LFP site was assigned to either contribute its trials to the low band or the

high band. The normalized, single-trial instantaneous beta amplitude was calculated (based on the Hilbert transform) for each band. We then adopted a Linear Model (LM) approach to determine which of the complementary task-related and spontaneous behavioral factors explained trial-by-trial amplitude variability in the two beta bands.

Low and high beta amplitude correlated differently with task-related and spontaneous behavior in single trials

The trial-averaged amplitude of the low band increased gradually after trial start and was maximal in the waiting period after SEL up to the valid SC. It then dropped following the valid SC and remained low through the remainder of the trial (Fig. 4B). The trial-averaged amplitude of the high band was strong through most trial epochs, right from the trial start. The amplitude decreased temporarily before and during the SCs. Both bands dropped to minimum amplitude during movement execution after GO.

Task-related and spontaneous behavioral variables were considered as regressors to explain the beta amplitude modulations. The task-related variables encompassed the color condition, the direction of the upcoming movement and the RT (monkeys had to initiate their movement rapidly). The spontaneous (uninstructed) variables included hand micro-movement velocity, eye velocity and gaze position. We also included a regressor representing the amount of time elapsed in the recording session ("time-on-task"; Stoll et al. 2015). The comparisons of the 247 models (combinations of 7 regressors and their 2-by-2 interactions) revealed that the winnings model, with the lowest Bayesian Information Criterion (BIC) in each 10ms bin along the trial, were mainly composed of a single or a combination of several non-interacting regressors (Fig. 4A). Interaction terms were present in the winning models in 37/1360 bins (there were 680 bins for each band) and were mainly interactions between the time-on-task and the eye gaze position (28/37 bins). The direction of the upcoming movement was almost always absent in the winning model except after the GO signal, around the

time of movement onset (and only for the low band). Consequently, 6 linear models, each including one relevant regressor, were fitted separately for the high and low beta bands.

First, we found that the color condition explained trial-by-trial variability of both beta bands (Fig. 4B, bottom). High beta band was modulated by the condition from the onset of SEL, and strongest around the spatial cues. The low beta band was modulated only from the onset of SC1. The condition had no effect before the onset of SEL, excluding any general effect of blocking of conditions on the beta activity.

This strong condition selectivity of both bands prompted us to also explore their modulations during the many distractor error trials. Indeed, when the monkey wrongly performed a reach towards one of the distractors, low and high beta amplitude profiles along the trial reflected the distractor selected by the animal (Suppl. Fig. 4A). In a decoding analysis, we trained a random forest estimator to decode color condition based on beta amplitude profiles in correct trials. We first tested the decoder on other correct trials, and for both the high and the low beta bands, the decoding was well beyond chance level (Suppl. Fig. 4B), but strongest for the low band. The decoder trained on correct trials could also decode the attended distractor in error trials (Suppl. Fig 4C) with the decoding performance again better for the low band, but also above chance level for the blue and pink conditions for the high band. The decoder was well below chance level in decoding the missed (valid) SC in distractor error trials (Suppl. Fig 4C). These decoding results confirmed that both low and high beta band amplitude modulations reflected the behavioral choices made by the animal, whether correct or wrong.

We next considered the normalized behavioral RT, as a measure of the level of reach movement preparation in individual trials. RT was strongly positively correlated with the low band amplitude, while almost no bin was significant for the high band (Fig. 5B). The correlation started immediately after the valid SC onset, and lasted up to the GO signal, however weaker for the blue color condition in the final delay before GO. Thus, from the onset of the cue that instructed the future movement, low beta amplitude was smaller in trials with shorter RT.

We then also considered the spontaneous eye and hand movements. First, the instantaneous eye velocity was poorly correlated with the high and low beta band amplitude (Fig. 4B, middle). Hand velocity, however, strongly explained the trial-by-trial variability of beta amplitude, but almost exclusively for the low beta band (Fig 4B, top). Low beta and hand micro-movement velocity correlated negatively during a majority of the trial and maximally after the onset of SC1 and the onset of SC2. The correlation was reduced in the final delay between SC3 and GO, in particular in the pink color condition. In order to understand the nature of this strong relationship between low beta amplitude and hand micro-movement velocity during the stable maintenance of central hold, we performed a covariance analysis (Fig. 5A). This analysis confirmed the strong negative correlation between hand velocity and low beta amplitude. It furthermore showed that the strongest correlation prior to valid SC onset was for beta *lagging* hand by about 100-130ms. After the valid SC onset, when low beta amplitude dropped (Fig. 4B), and subsequently hand velocity increased (Fig. 1C), the covariance analysis showed a widening in the cross-correlation, with maximal negative correlation for 260-270ms in the direction of beta *leading* hand.

The strong correlations with both RT and hand micro-movement velocity for low beta amplitude prompted us to explore whether hand micro-movements were directly predictive of RT. We correlated hand velocity with RT across all trials in all sessions, in 10ms bins along the trial. However, this correlation was weak and only rarely significant prior to the GO signal (Suppl. Fig. 5).

After observing that eye velocity did not explain beta amplitude variability, we explored to which degree gaze direction modulated beta amplitude. Both monkeys spent a considerable fraction of each trial with the gaze directed away (Out) from the work area (Fig. 1E-F), possibly reflecting moments with less focal attention on the task. We quantified the correlation between gaze position (In/Out of the work area) and high and low beta amplitude at various lags. A lag with gaze *leading* beta by 230ms resulted in the largest number of correlated bins for both bands (Suppl. Fig. 6B). At this lag, the high beta band amplitude was strongly modulated by gaze position in particular in the trial epochs preceding the valid SC onset, and again just before the GO signal. In moments with gaze

In, high beta amplitude was higher, in particular during the delays. The temporary decrease in amplitude at the valid SC had similar amplitude for gaze In/Out. Thus, the rhythmic modulation in high beta amplitude by the rhythmic task event was largely abolished when considering only time-points with gaze Out. Considering gaze position at zero lag, or a lag in the opposite direction (as beta leading gaze) largely abolished the strong high band amplitude modulations due to gaze position (Suppl. Fig. 6A). Gaze position also influenced low beta band amplitude (Fig. 6A). However, the effect was variable, with some bins having larger amplitude for gaze In, and others for gaze Out of the work area (Fig. 6B). The most consistent effect across the three color conditions was a delay in the drop of beta after thevalid SC onset for gaze Out, and increased amplitude prior to GO for gaze In. We further explored the effect of delayed low beta amplitude drop after the valid SC for the gaze Out position. We split trials according to gaze position at exactly 200ms after the valid SC onset, and plotted low beta amplitude for all trials with gaze either on the target (valid SC), inside the work area but not on the target, or outside of the work area (Suppl. Fig 6C). This confirmed that the decrease in beta amplitude mainly occurred for trials with gaze In (on the target or otherwise inside the work area), compared to trials with the gaze still Out.

Finally, for both beta bands, amplitude increased systematically within the behavioral session (time-on-task). For the high band, the amplitude increase for late trials was particularly strong during SEL, and in the delay immediately preceding the valid SC, but also in other task epochs. For the low band, amplitude increased significantly within the session in most trial epochs, both before and after the valid SC onset. A supplementary spectral parametrization analysis (Donoghue et al. 2020) confirmed that this increase was specific to the two beta bands and not caused by a change in the overall level or the slope of the aperiodic signal, which remained unchanged (Suppl. Fig. 7).

DISCUSSION

We here describe a double-dissociation in sources and behavioral correlates of motor cortical low and high beta, with respect to both task-instructed and spontaneous behavior. In two macaques performing a delayed visuomotor reaching task, low beta dominated in M1, while high beta dominated in PMd. Low beta correlated positively with RT during preparation and negatively with uninstructed hand postural micro-movements throughout the trial. In contrast, high beta was unrelated to RT and hand postural dynamics, and instead was selectively modulated in anticipation of and during visual cues, thus reflecting temporal predictions. However, this modulation was largely abolished when the gaze was oriented away from the work area. These clear-cut differences reconcile the many disparate roles proposed for the broader beta rhythm (~13-35Hz), and designate specific roles in movement control for M1 low beta and spatio-temporal attention for PMd high beta.

Behavioral task performance and spontaneous movements

The monkeys performed a rule-based and predictive visual cue selection task entailing strong working memory components, first for selecting the valid spatial cue (target) based on a color matching rule, and second to memorize the target position while preparing the reach. Both monkeys had increased performance for the condition in which the last of the three sequentially presented cues was valid. This might be because this cue was closer in time to the GO signal, requiring working memory for target location for a shorter duration. However, it could be that visual distractors occurring during movement preparation and while the target location was kept in working memory were more distracting in the two other conditions. Monkey M, who had the largest increase in performance when the third spatial cue was the valid one also gazed more towards the cue indicating the valid color (SEL) in that condition (Fig. 1F). Thus, there was possibly a behavioral bias in in favor of this (easier) condition from the trial start.

Both monkeys performed uninstructed (spontaneous) hand and eye movements that were aligned to the task events. Such spontaneous movements persist even in highly constrained settings

(Tremblay et al. 2022). Our monkeys were head-fixed, but free to move their eyes. Furthermore, they had to maintain their hand position within a very limited zone through most of the trial. Yet, they frequently made micro-movements with the hand, in particular during movement preparation. These spontaneous movements did not have any directional bias reflecting the planned movement, but possibly resulted from increased postural muscle tonus during movement preparation (Suppl. Fig. 1E) being imperfectly balanced across different muscles. As we discuss below, the neuronal activity was correlated with these spontaneous hand and eye movements to a similar degree as with the task-instructed behavior.

Low beta dominates in M1 and high beta dominates in PMd

We found low beta to dominate in M1, while high beta dominated in PMd. Rather than a gradual shift in peak frequency of a single beta band along the posterior-anterior axis, we observed two distinct bands also at intermediate sites. Most studies of sensorimotor beta rhythms in monkeys lumped frequencies from ~13-35Hz, such that any gradient across cortex might have been overlooked. However, consistent with our result, Chandrasekaran et al. (2019) found beta peak frequency in PMd to be above 20Hz, whereas near the central sulcus (including M1 and somatosensory areas) beta was mainly observed to peak at or below 20Hz (Rouguel et al. 1979; Courtemanche and Lamarre 2005; Witham and Baker 2007; Witham et al. 2007; Haegens et al. 2011; Zanos et al. 2018; but see also Baker et al. 1999, Peles et al. 2020). Several studies of beta rhythms in monkey prefrontal cortex reported peak frequencies above 20Hz (e.g. Buschman and Miller 2007; Buschman et al. 2012; Lundqvist et al. 2016; Haegens et al. 2017; Rassi et al. 2022). Furthermore, Vezoli et al. (2021) found high beta to be dominant anterior to low beta across the fronto-parietal cortex in macaque ECoG, while Mahjoory et al. 2020 reported a gradual increase in beta peak frequency along the posterior-anterior axis in human resting state magnetoencephalography. It is therefore probable that the low and high beta bands that we here characterize across motor cortex extend well beyond, and at the cortical level reflect a low beta network including M1, somatosensory

and parietal regions and a high beta network including PMd and prefrontal regions, not excluding the involvement of also sub-cortical structures (e.g. Courtemanche et al. 2003; Courtemanche and Lamarre 2005; Feingold et al. 2015).

We analyzed single-trial continuous beta amplitude variations, rather than signals binarized into epochs with and without bursts using an arbitrary threshold. This facilitated the use of a Linear Model (LM) framework to correlate beta amplitude to the task and behavioral factors at the single trial level, in a time-resolved manner. The two beta bands modulated very differently in relation to the predictable temporal structure of each trial. The amplitude in the low band split for the three color conditions only after the onset of SC1, in a 'reactive' manner which could reflect movement preparation. In comparison, the amplitude of the high band was already selective after the onset of SEL, in anticipation of the SCs. The condition selectivity found with the LM analysis was supported in a decoding analysis. The decoder trained on correct trials could also decode (above chance level) the spatial cue that was used by the animal in distractor error trials. Thus, the beta amplitude modulations reflected the actually attended cue, and not the cue that should have been attended.

Low beta reflects movement preparation and continuous postural dynamics

A decrease in sensorimotor beta amplitude during preparation, as we found for low beta, was already observed in many studies (Kilavik et al. 2013). The selective decrease in amplitude of the low band following the valid spatial cue, the moment-to-moment negative correlation with spontaneous hand micro-movements and the positive trial-by-trial correlation with behavioral RT during the preparatory period are strong evidences in favor of a role for beta in postural control and movement preparation (Salmelin et al. 1995; Conway et al. 1995; Baker et al. 1999; Brown 2000; Engel and Fries 2010; Jenkinson and Brown 2011; Perfetti et al. 2011 ; Pastotter et al. 2012 ; Khanna and Carmena 2017; Chandrasekaran et al. 2019 ; Peles et al. 2020). Specifically, this concerns the low beta band dominating in M1. In contrast, the amplitude of the high beta band in PMd was independent of hand micro-movements and behavioral RT, and did not remain low during movement preparation. The

correlation between low beta and RT (Fig. 5B) started several seconds before the GO signal, as also observed for motor cortical visual evoked potentials (Kilavik et al. 2010). The correlation can even be present before stimulus onset in visual RT tasks (e.g. Zhang et al. 2008; Buschman et al. 2012; Chandrasekaran et al. 2019). Thus, visual cue processing in early stages of preparation is important for optimizing movement performance. We found no correlation between low beta amplitude and RT before the onset of the valid spatial cue. RT variability was therefore most likely related to variability in movement preparation processes, and not to general arousal.

A recent study reported transient beta bursts even during sustained isometric gripping in humans (Echeverria-Altuna et al. 2022), suggesting no direct moment to moment link between cortical beta amplitude and motor output. The postural micro-movements we observed were a 100-fold smaller in velocity than the center-out reach responses (Suppl. Fig 1A), yet strongly correlated with low beta amplitude across all trial epochs. The discrepancy between our findings and theirs could be due to the large number of trials available for our analysis from collapsing all LFP sites, or possibly to less sensitivity in their setup for detecting minute changes in grip force during the sustained isometric contraction.

The negative correlation between low beta and hand velocity was maximal at temporal lags of 100-130ms (beta *lagging* hand) prior to the valid cue onset (Fig. 5). In comparison, directed descending and ascending coherence in the beta frequency range between cortex and muscle (Witham et al. 2010, 2011) were reported to have much shorter phase delays than this, on the order of 25ms. Jasper and Penfield (1949) already speculated whether the emergence of sensorimotor beta bursts reflected entering a state of neuronal population dynamics equilibrium, with beta being a network resonance frequency (see also Jensen et al. 2005; Rosanova et al. 2009; Lundqvist et al. 2020; Mahjoory et al. 2020; Chota et al. 2023). A decrease in M1 low beta amplitude, in response to hand postural micro-movements could reflect a temporary shift away from equilibrium with the aim to stop further displacement of the hand cursor outside the central fixation spot, which would have aborted the trial. However, beta lagged the hand also at trial start, when residual hand movements

related to the placement of the hand cursor within the central fixation spot were still prevalent. Thus, these low beta amplitude modulations could also reflect some form of post (micro-)movement beta rebound.

During movement preparation the average low beta amplitude started to decrease a few hundreds ms before the average hand velocity started to increase. The trial-by-trial cross-correlation showed that in this trial epoch low beta amplitude and hand velocity correlated negatively across a broad range of lags, with maximal correlation strength for beta *leading* the hand of about 260-270ms. This could reflect the average difference in onset of the changes in these two signals in response to the valid cue. Tremblay et al. (2022) showed that uninstructed movements could be informative about task-related behavior. However, in our case, the hand micro-movements did not predict behavioral RT, which also correlated strongly with low beta amplitude during movement preparation. In conclusion, low beta reflects multiple components of motor control simultaneously, that between them are largely independent.

High beta reflects temporal task prediction and focal attention

Rhythmic modulations in average beta amplitude in frontal cortex were observed in several studies using rhythmic visuomotor or working memory tasks (Saleh et al. 2010 ; Lundqvist et al. 2016) or passive auditory tasks (Fujioka et al. 2012) permitting temporal predictions. Furthermore, beta amplitude scaled to predictable delay durations (Kilavik et al. 2014; Sun et al. 2021). We found that temporal prediction and attention only affected the high beta band dominant in PMd. Notably, high beta amplitude was already strong at trial start (central touch), and modulated selectively after SEL, which indicated the color to be attended. Thus, whereas the selectivity in the low band only emerged during movement preparation, the high band was selective in anticipation of the spatial cue.

Neither of the two beta bands modulated in amplitude in relation to eye velocity, which is not surprising since we recorded in regions coding for upper limb movements. However, the high band was strongly modulated by gaze direction (In/Out of the work area) in particular prior to the

449 presentation of the valid cue (Fig. 6). The overall amplitude of high beta and the rhythmic modulation
450 around visual cues were much stronger when considering the time points in each trial with the gaze
451 directed towards the work area. The effect was maximal when the gaze position was considered
452 about 230ms in the past, with respect to the high beta amplitude (Suppl. Fig. 6). Thus, gaze position
453 conditioned future high beta amplitude. We interpret this in relation to spontaneous switches
454 between covert attention (gaze Out) vs. overt or focal attention (gaze In). Trial start and GO were
455 more than 6s apart, which is very long for maintaining focal overt attention. Having the gaze out of
456 the work area, which was more frequent before the valid cue presentation (Fig. 1E-F), probably
457 reflected less focal attention on the visual scene. This decreased the rhythmic modulations in high
458 beta amplitude and notably the maxima during the delays prior to the valid cue onset. The temporal
459 predictability of the task events permitted shifting the gaze to the work area in anticipation of or
460 triggered by salient visual events, in particular the valid cue. This probably explains why the
461 performance was correct even with periods in the trial being performed with peripheral vision and
462 less focal attention. Having the gaze Out affected low beta amplitude notably by delaying the
463 decrease in amplitude following the valid cue. Thus, less focal attention on the visual scene possibly
464 delayed the onset of movement preparation.

465 The rhythmic modulation we observed in high beta amplitude resembled strongly the one
466 reported by Lundqvist et al. (2016) for prefrontal cortex (PFC) during a working memory task
467 requiring central eye fixation. We verified that the high beta band recorded in the PMd sites was
468 locally generated by assessing locking of local neuronal spiking to beta phase. It is however likely that
469 the high beta band is generated in a larger network also including the PFC. The similarity of the high
470 beta band modulations in the two studies suggests that reflections of (rhythmic) temporal
471 predictions of visual cues are prevalent in moments of increased focal overt attention. Combined,
472 this supports a role for PMd high beta in sensorimotor spatio-temporal prediction and attention (e.g.
473 Murthy and Fetz 1992, 1996; Sanes and Donoghue 1993; Rubino et al. 2006; Androulidakis et al.

2006; Lalo et al. 2007; Saleh et al. 2010; Fujioka et al. 2012; Kilavik et al. 2014; Wiener et al. 2018; Sun et al. 2021).

Time-on-task effects on low and high beta

High beta in frontal cortex was shown to increase in amplitude from early to late within behavioral sessions, possibly reflecting increased attentional effort or fatigue (Stoll et al. 2015). We therefore included the time spent on the task as a regressor in the LM analysis. It affected strongly the amplitude of both bands (Fig. 7), but not the aperiodic signal component. For the low beta band, the time-on-task effect was present across all trial epochs. For the high band the effect was particularly strong during the SEL cue presentation, and in a condition selective manner in the delay immediately preceding each valid cue. This could suggest that late in the session, there was overall increased postural control as reflected by increased low beta amplitude, but also increased focal attention in anticipation of and during to the most relevant visual cues (SEL and valid SC), as reflected by the high beta modulations.

Conclusion

Beta oscillations in sensorimotor cortex remain enigmatic, almost 75 years after the first descriptions and interpretations were offered by Jasper and Penfield (1949). We proposed more than 10 years ago that by considering small, yet systematic frequency changes within a broader beta band, more insight can be gained regarding trial-by-trial and epoch specific correlates of sensorimotor beta band rhythms (Kilavik et al. 2012). Since then, the analysis of time-resolved beta amplitude at the single trial level, also by quantifying different parameters of individual bursts has become the gold standard, holding the promise to considerably advance our understanding of sensorimotor beta (Zich et al. 2020). By designing a demanding visuomotor task, and by monitoring task-related, and also spontaneous behavior, we here describe a double-dissociation in cortical sources and behavioral correlates of low and high beta in motor cortex. These clear-cut findings reconcile the largely disparate roles proposed for sensorimotor beta, ranging from, on the one extreme, movement

inhibition, and on the other extreme, temporal expectation (reviewed in Kilavik et al. 2013). Only by acknowledging that motor cortex contains multiple beta rhythms, each with specific behavioral and cognitive correlates, can we advance towards a complete understanding. In this perspective, our study is an important step forward.

MATERIALS AND METHODS

Animal preparation

Two adult male Rhesus monkeys (T and M, 10 and 14 kg, respectively) participated in this study. Care and treatment of the animals during all stages of the experiments conformed to the European and French Government Regulations (2010/63/EU; authorization identifier 03383.02). Previously published studies using data from these two monkeys (Kilavik et al. 2010, 2012, 2014; Ponce-Alvarez et al. 2010; Confais et al. 2012, 2020) were based on recordings from the opposite hemisphere during performance of another visuomotor task.

Subsequent to learning the visuomotor task (see below) the monkeys were prepared for multi-electrode recordings in the left hemisphere of the motor cortex (M1 and PMd), contra-lateral to the trained arm. In a first surgery, prior to completed task learning, a titanium head-post was implanted posteriorly on the skull, fixated with titanium bone screws and bone cement. In a second surgery, several months later, a cylindrical titanium recording chamber (19mm inner diameter) was implanted. The positioning of the chamber above upper-limb regions of M1 and PMd was confirmed with T1-weighted MRI scans (prior to surgery in both animals, and also post-mortem in monkey M), and with intra-cortical electrical micro-stimulation (ICMS; as described in Asanuma and Rosen 1972) performed at the end of single-tip electrode recording days in the first recording weeks, in both monkeys (Fig. 3C). The recording sites included in this study spanned about 15mm across the cortical surface in the anterior-posterior axis, and only include sites determined with ICMS to be related to upper limb movements. The exact border between PMd or M1 areas was not estimated.

Behavioral setup and task

Two monkeys were trained to perform a visuomotor rule-based and predictive cue-selection task (Fig. 1B). The task required arm-reaching responses after a GO signal, in one of 4 (diagonal) directions from a common center position, performed by holding a handle that was freely movable in the two-dimensional horizontal plane. The visual scene was displayed on a vertical computer

monitor (LCD; 75 Hz) in front of the monkey (Fig. 1A). We here describe the monitor stimuli in cm units, but since the viewing distance was about 57 cm, this approximates to the same degrees of visual angle. Before the start of each trial, the monitor displayed the handle (hand cursor) position (small white square; 0.4cm edges), a central fixation spot (yellow flickering disc; 0.45cm radius), and the 4 possible peripheral target positions (red circular outlines; 1.5cm radius at 9 cm diagonal distances from the center). The position of the cursor was updated on the monitor every 40ms (~every 3rd frame), but only if the accumulated displacement from the previous update exceeded 0.1cm (to avoid flickering position due to electronic noise).

The monkey initiated the trial by positioning the cursor inside the central hand fixation spot. This central touch ended the flickering of the fixation spot (which remained on), and was accompanied by an auditory tone, presented for 50ms. After holding this central position for 1000ms, a selection cue (SEL) indicating the color rule for that trial appeared on the screen for 300ms, displayed behind but extending well beyond the central yellow disc and the overlying hand cursor. SEL consisted in one out of three differently colored polygons (blue, green or pink; ~3cm radius) defining the trial type. A 1000ms delay followed SEL offset. Thereafter, three peripheral spatial cues (SC1-3) were presented in sequence, each displayed for 300ms, with 1000ms delay after each of them. The SCs were colored discs (0.9cm radius), always presented in the temporal order blue-green-pink, each within one of the 4 peripheral red outlines.

All 4 diagonal target positions were equally likely for each SC. Thus, successive SC in the same trial could be presented in the same position. This resulted in 192 unique conditions, combining the 3 trial types (color rule) with the 4 independent positions for SC1, SC2 and SC3. In monkey T, who was not willing to work for as many trials as monkey M, only 3 of the 4 target positions were used in each session (randomly selected for each session), in order to reduce somewhat the number of unique conditions. For both animals, in order to ease the task, the three trial types (i.e. color rule) were presented separately in small blocks of approximately 15 unique conditions per block, cycling across multiple blocks of the three trial types to complete all the unique conditions. The unique conditions

within each block were presented in pseudo-random order. Incorrect trials within a block were re-presented later in the same block, and each block was completed only when all unique conditions in the block were correctly executed.

The animal had to select the (valid) SC according to the color rule indicated by SEL (i.e. delayed color match to sample), and ignore the two (distractor) SCs of different colors. The GO signal was presented after the final 1000ms delay following SC3, prompting the animal to execute the center-out arm reaching movement to the memorized target position indicated by the valid SC. The GO signal was directionally non-informative, consisting in the simultaneous onset of 4 red light-emitting diodes (LEDs; embedded in a thin Plexiglas plate in front of the monitor) at the centers of the 4 circular target outlines. The reaction time (RT) and movement times each had a maximum allowance of 500ms. The animal was trained to stop and 'hold' within the correct peripheral target outline for 300ms to obtain a reward. The moment of onset of valid target touch was signaled by an auditory tone (50ms) and a completed hold with another tone (50ms). Reward was delivered 500ms after completed hold, and consisted in a small drop of liquid (water or diluted fruit juice). Monkey T was not rewarded for non-hold trials, while monkey M was given a smaller reward on non-hold trials (on the valid target; 500ms after breaking hold). For both animals, these non-hold trials were included in the analysis (about 10% of all included trials).

The manual work area of the monkey was scaled down with respect to the display on the monitor (by a factor of about 0.7). Thus, the diagonal distance (center to center) between the fixation spot and peripheral targets was 6.5cm. The required central fixation zone was defined to be within a radius of 0.3cm, and the accepted touch zone of the peripheral targets had a radius of 1cm. These touch zones corresponded to the hand cursor overlapping more than halfway with the fixation spot or the peripheral outlines, respectively. In the offline analysis of the hand signal, we used the spatial scaling of the visual scene on the computer monitor.

In short, in this rule-based and predictive cue-selection task, the timing and sequential order of the three SCs were predictable, and SC validity was indicated at the start of each trial by SEL. Only the spatial positions of the three SCs were unpredictable.

Data acquisition

During recording days (maximally 5 days a week), a multi-electrode, computer-controlled microdrive (MT-EPS, Alpha Omega, Nazareth Illith, Israel) was attached to the recording chamber and used to transdurally insert up to five single-tip microelectrodes (typical impedance 0.3-1.2MΩ at 1,000Hz; FHC) or up to two linear microelectrode arrays (either V- or S-probes, Plexon, Dallas, TX, USA or LMA, Alpha Omega; each with 24 or 32 contacts, inter-contact spacing either 100, 150 or 200µm; 12.5 or 15µm micrometer contact diameters) into motor cortex. In this study we employ the term 'site' for the recording obtained from each individual single-tip electrode (or from each linear array) recorded in individual behavioral sessions. The electrodes (or arrays) were positioned and lowered independently within the chamber (Flex-MT drive; Alpha Omega) in each session. Individual guide-tubes for each electrode/array were used that did not penetrate the dura (no guide was used for the more rigid LMA array). For single-tip electrodes, the reference was common to all electrodes and connected, together with the ground, on a metal screw on the saline-filled titanium recording chamber. For the linear array recordings, the reference was specific to each array type. For the LMA (Alpha Omega) it was an insulated wire exposed at the tip, either emerged in the chamber saline, or attached with crocodile clip to the probe stainless steel tube (which in turn was lowered into the chamber liquid, but not extending into brain tissue). For the V- and S-probes (Plexon) in most cases the references was the stainless steel shaft of the array (extending into brain tissue, in near proximity to the probe's recording contacts). In a few sessions, the references was instead placed on a skull-screw on the more posterior headpost (7/41 sites using v-probes in monkey T) or on a screw on the saline-filled recording chamber (1/51 sites using s-probes in monkey M). For both array types, the

ground was either connected to a skull-screw of the remote titanium head-fixation post, or to a screw of the titanium recording chamber.

We used two different data acquisition (DAQ) systems to record neuronal and behavioral data. All single-tip electrode recordings in monkey T were obtained on a recording platform with components commercialized by Alpha Omega. This system included the Alpha-Map system for online monitoring of signals (running on Windows XP), and the MCP-Plus multi-channel signal processor including analog head-stages. Neuronal signals from each electrode were amplified with a gain of 5,000 to 10,000 (with unit-gain head-stage), hardware filtered (1Hz – 10kHz) and digitized and saved for offline analysis at a sampling rate of 32 kHz.

All linear array recordings in monkey T, and all recordings (single electrodes and linear arrays) in monkey M, were obtained on a recording platform with components commercialized by Blackrock Neurotech (Salt Lake City, UT, USA). This system included Cereplex M digital head-stages (versions PN 6956, PN 9360 and PN 10129) connected to a Digital Hub (versions PN 6973, PN 6973 DEV 16-021, PN 10480) via custom HDMI cables (versions PN 8083, PN 8068), which transmitted signals via fiber optics to a 128 channel Neural Signal Processor (NSP hardware version 1.0), and control software Cerebus Central Suite (v6.03 and v6.05 for monkeys T and M, respectively; running on Windows 7). An adapter (PN 9038) permitted connecting multiple single-tip electrodes to the Cereplex M Omnetics connector (Monkey M). Neuronal signals were hardware filtered (0.3Hz – 7.5 kHz) and digitized and saved for offline analysis at a sampling rate of 30 kHz.

Behavioral event codes (TTL, 8 bits) were transmitted online to the DAQ system from the VCortex software (version 2.2 running on Win XP; NIMH, http://dally.nimh.nih.gov), which was used to control the behavioral task. A custom rebuild of the VCortex software allowed simultaneous online monitoring of hand and eye gaze positions in the common reference frame of the animal's visual monitor display. Continuous hand position (X and Y) was obtained from two perpendicularly superimposed contactless linear position magnetorestrictive transducers, model MK4 A; GEFRAN, Provaglio d'Iseo, Italy). The 'floating' magnetic cursor was attached to a manipulandum that could be

633 moved along two pairs of rails with ball bearings, each pair aligned with one of the two transducers.
634 The Y-oriented rails were fixed on top of the X-oriented rails. As such, this system provided
635 somewhat less frictional resistance in the Y direction than in the X direction. Furthermore, either of
636 the uni-directional X or Y displacements provided somewhat less frictional resistance than their
637 combination needed to move to the diagonally placed targets. Hand position was used online to
638 control the behavioral task. The hand position was also saved by VCortex for offline analysis (at
639 250Hz sampling rate). In a majority of sessions, eye gaze position (X and Y) was recorded by the DAQ
640 system (video based infrared eye-tracking; RK-716PCI (PAL version) at 50Hz for the first single-tip
641 electrode recordings in monkey T, or ETL-200 at 240Hz sampling rate for the array recordings in
642 monkey T and all recordings in monkey M; ISCAN Inc., Woburn, MA, USA). The eye-tracking camera
643 was positioned next to the lower right corner of the monkey's computer monitor.
644 In many sessions we also recorded heart rate (plethysmographic pulse waveform from ear-clip
645 pulse oximeter, model 8600V; Nonin Medical Inc, Plymouth, MN, USA), and in some sessions surface
646 electromyogram (EMG) from one or two proximal upper limb muscles (deltoid/biceps).
647
648 **Hand position analysis**
649 All analyses of behavioral and neuronal data were conducted offline by using Matlab (The
650 MathWorks, Inc.).
651 The hand position signals that were recorded with VCortex were realigned in time with the other
652 data recorded by the DAQ system offline, by realigning the behavioral event codes and up-sampled
653 (linear interpolation) from 250Hz to 1kHz. The hand position signals were calibrated (scaled) online in
654 the VCortex configuration to match the visual display before storing on file, and in analysis we used
655 the spatial scaling of the visual scene in cm.
656 The RTs for the center-out reaching movements were redefined offline using the hand
657 trajectories. First, hand velocity and acceleration were computed in each trial, using a Savitsky-Golay
658 algorithm. To determine reach movement onset, in a 2000ms duration epoch centered on GO,

659 periods with prolonged increased velocity (>50ms) above an empirically determined velocity-
660 threshold (6 cm/s) were then detected, and the final, preceding increase in acceleration above an
661 empirically determined acceleration-threshold (6 cm/s/s) was then taken as the time of movement
662 onset. These RTs were confirmed in both animals by visual inspection of single trial trajectories in
663 several sessions.

664 We also quantified hand micro-movements during the maintenance of stable central hand
665 position using hand velocity and position.

666

667 **Eye position offline calibration and analysis**

668 In a majority of sessions we recorded eye position with an infrared camera. A rough online
669 calibration of the gain and offset of the eye X and Y signals were done during the first behavioral
670 trials in each recording session, to compensate for small changes in head fixation or camera position
671 compared to the previous day/session. This simplified online calibration was adopted to avoid
672 training the monkey in a fixation task. The center of gaze was set to zero (center) while the monkey
673 looked at the small yellow central target in order to place the hand cursor therein to initiate a new
674 trial. Then, on some days the X or Y gain was updated slightly so that the spontaneous eye fixations
675 on the peripheral target outlines matched their position in the Cortex software interface. The trials
676 before calibration (typically 0-3 correct trials) were excluded in offline analysis involving eye
677 movements.

678 For data analysis, the eye signals recorded with the DAQ system were re-calibrated offline, to
679 correct for the distortion induced by having the camera off the horizontal and vertical central axes of
680 gaze. First, the raw eye signals were inspected visually to exclude from offline calibration and analysis
681 the trials that were recorded before the completion of the rough online calibration, typically
682 consisting in suppressing the 0-3 first correct trials in each session. Raw data were downsampled
683 from the acquisition sampling frequency (1 or 30 kHz) to the camera sampling frequency (50 or
684 240Hz) and linearly rescaled from bits to volts. We computed the eye velocity in volts/s using the

685 Savitzky-Golay algorithm. For the offline calibration algorithm, we only considered data points that
686 likely belong to fixation periods (i.e. whose velocity was lower than the lower 10th percentile of the
687 total velocity distribution). At this stage, the superimposition of eye positions during these slow
688 velocity epochs across all trials in a session already showed an expected clustering of the data around
689 5 positions on the screen whose geometry resembled the center and 4 peripheral target positions
690 used in the task. Thus, we were able to define boundaries in the voltage space to separate data
691 points according to whether they were recorded when the monkey was looking within the work area
692 (approximate boundaries of computer monitor) or when he was looking away from the work area
693 (e.g looking in the ceiling, or signal saturation due to eye blinks). The slow velocity (fixation) data
694 occurring within the work area was then sorted into 5 clusters using a k-means algorithm (kmeans
695 function in MatLab, using squared Euclidean distance). Cluster centers were assumed to represent
696 the target positions in the voltage space. We next generated a 2D non-linear model to compensate
697 for the distortion due to camera position, between target coordinates on the screen (in cm) and
698 voltage amplitudes of the corresponding centroids. This was achieved by adjusting a polynomial
699 function to fit the relationship between each coordinate in the screen space to the XY coordinates in
700 the voltage space. The correction was then applied to the complete eye traces. A detailed version of
701 this correction can be found in DeHaan et al. (2018). Each data point was re-assigned to a cluster if it
702 was located at a distance <2cm from the target's center coordinates, or assigned as being between
703 clusters (but within the work area), or outside of the work area (incl. saturated). Eye position,
704 velocity and acceleration were then saved for further analysis, scaled in cm of the visual display,
705 alongside cluster membership of each data point. Furthermore, the data points outside the work
706 area that were beyond the lower or upper 0.99 percentiles of the boundaries of the raw X and Y
707 voltage signals were marked as 'saturated'.

708 To detect the saccadic eye movements, we applied a recursive algorithm that seeks for the largest
709 breakpoint in a piecewise stationary process, in a trial-by-trial fashion. First we computed the
710 cumulative 2D velocity of the eye signal in cm/s. This representation yields a pseudo staircase profile

alternating between steep and slowly increasing periods over time. We extracted the highest decile of the velocity distribution and marked the corresponding steps in the staircase as boundaries to define periods when the subject was looking coarsely in the same area. These steps corresponded to blinks or to obvious large saccades and the steady periods were either fixation periods or multiple fixation periods with intermittent smaller saccades. During the steady periods, the cumulative distribution showed a slow increase due to noise originating from micro-movements and the recording device. The contribution of this noise being dependent on the location of the fixation on the screen, we compensated for it by subtracting the average slope for each period separately. This gave a piecewise stationary process that showed pseudo-horizontal steady epochs with better signal to noise ratio for the intermittent smaller saccades. Secondly, we applied a recursive algorithm to this process consisting, within a given time window, to compute at each data point the difference between the prior and the posterior average values. The maximum difference was extracted and compared to a threshold value computed after the velocity profile of a reference saccade (10ms duration, 60cm/s velocity peak). If the maximum difference was larger than the threshold, it was considered an actual transition and the time window was split in two at this timepoint. Starting with a time window covering the whole trial, the algorithm defined new (smaller and smaller) time windows at each iteration and the new window boundaries were considered as transitions. To avoid transitions to be detected multiple times, we introduced a 'refractory period' of +/-15ms around accepted transitions. Fixation periods were finally defined by sorting the transitions between fixations into detected saccades or detected micro-saccades depending whether or not the euclidian distance between the isobarycenter of two successive fixations was larger than a threshold (the change in eye position on the screen for an eye movement of 0.5cm). Saccade onset/offset times were saved for further offline analyses alongside the other calibrated eye signals detailed above.

Finally, eyeblinks were detected as two subsequent (<150ms apart) eye signal velocity passings beyond a velocity threshold (500cm/s for the 50Hz sessions and 800cm/s for the 240Hz sessions). The data points in a window including the gap between these subsequent threshold passings, as well

as a couple of preceding and subsequent flanker datapoints were marked as eyeblinks. Visual inspection confirmed that this method was able to distinguish between saccades and abrupt velocity increases due to eyeblinks, even if large standalone saccades sometimes had velocities beyond the thresholds used for eyeblink detection.

LFP spectral analysis and beta amplitude extraction

All sessions with sufficient quality of data were included in analysis. The raw signals were low-pass filtered offline at 250Hz cut-off frequency (zero-phase 4^{th} order Butterworth filter, using the butter and filtfilt functions in Matlab) to obtain the LFP signal, which was then downsampled to 1KHz and saved for further analysis. For this study, we included only one contact for each of the linear array penetrations, selected to be well within cortex and with low noise (e.g. no heartbeat artifacts). LFP activity from 110 individual sites (63 with single-tip electrodes and 47 with linear arrays) in 59 sessions monkey T and 60 sites in 39 sessions (10 with single-tip electrodes and 50 with linear arrays) in monkey M were included in the analysis. A site is here defined as the conjunction of a specific chamber coordinate of the electrode entry and cortical depth, in one recording session. In the included LFP sites, trials with obvious artifacts (mainly due to teeth grinding, static electricity or heart-beat signal) detected by visual inspection, were excluded from further analysis (12.3% of all trials in monkey T and 5.1% in monkey M). As the duration for which the monkeys were willing to work varied across sessions, after trial exclusion, the analyzed sites included on average 96.4 +/- 48.8 (STD) trials (range 19-184) in monkey T, and 147.3 +/- 80.3 trials (range 18-281) in monkey M. We included also the sites with few trials, since a majority of the neuronal data analyses were done on trials grouped across many sites.

Power spectral density (power for short) estimates of the LFP were obtained using the pwelch function of Matlab. For LFP spectrogram examples (Fig. 2A-C), we first highpass filtered the LFP with 3Hz cutoff, using a 4th order Butterworth filter. Power was estimated for single-trial sliding windows of 300ms duration, with 50ms shifts, at 1Hz resolution, before averaging across trials.

For average spectrograms for each monkey (Figs. 2E and 3D), we also used 300ms sliding windows, 50ms shifts, at 1Hz resolution. For each individual LFP, we first highpass filtered the signal (3Hz cutoff, 4th order Butterworth filter), before calculating the power for each window in single trials. Next, the power matrix (trial x window x frequency) for each LFP was normalized by dividing by the mean power between 10-40Hz across trials and windows for that LFP. We then computed for each window the grand average power across all individual trials for all normalized LFPs (i.e. each trial contributed equally to the grand mean, independent on the total number of trials for the specific LFP site). For single site and average spectrograms we used a perceptually flat color-map (Crameri 2018), with color limits set to the minimum and maximum power values between 12-40Hz between onset of SEL and GO, separately for each site or each monkey.

To determine the peak frequencies of the two observed beta bands, we estimated power in a 900ms epoch preceding SC1 onset, across all trials for each LFP site (after initial highpass filtering at 3Hz ; 4th order Butterworth filter). Within this epoch, we used five 500ms windows, with overlap of 400ms, to get one average power estimate per trial. Before plotting the grand average spectral power (Fig. 3A), we normalized the PSD matrix (trial x frequency) for each LFP by dividing by the mean power across trials between 10-40Hz for that LFP. We also determined, for each individual trial, the frequency between 10 and 40Hz with maximal power, to plot the distributions of (beta) peak frequencies across all trials and LFP sites for each monkey (Fig. 3A). Based on these distributions, for both monkeys a frequency range for the low band of 13-19Hz and for the high band of 23-29Hz were used to determine the dominant beta band for each LFP site. We computed a beta band dominance index using mean power across all trials and frequencies in the low band minus mean power across all trials and frequencies in the high band, divided by the sum of the two. Significance in band dominance was determined with a paired t-test across trials, taking the mean power across all frequencies in each band for each trial (Fig 3C).

To separate the aperiodic and periodic components of the signal (Suppl. Fig. 7), for each monkey we performed spectral parametrization with the FOOOF method (Donoghue et al. 2020) in the pre-

789 SC1 period in blue trials. We split trials according to whether they were performed early or late
790 within a session. Trials were labeled as 'early' when belonging to the first third of each session and
791 'late' when belonging to the final third. The aperiodic component was fitted with a frequency range
792 of 5-194Hz, using the 'knee' mode.
793
794 **Phase-locking of neuronal spiking to LFP beta phase**
795 To verify that the LFP beta oscillations were at least partially of local origin, we analyzed phase-
796 locking of the simultaneously recorded neurons to the LFP beta phase of the site-dominant band. We
797 included only the laminar recording sites, and tested phase locking for neurons across all laminar
798 contacts to the LFP on the selected LFP contact on the same laminar probe, to ensure proximity of
799 the two signals. We analyzed the pre-SC1 delay, since the beta amplitude was generally strong in
800 both animals and in both bands in this delay. Only neurons with more than 100 spikes in this delay,
801 accumulated across all trials, were included. Beta phase was extracted from the Hilbert
802 transformation of the beta-filtered LFP, only for the dominant beta band at each LFP site, and the
803 phase at each spike time was determined.
804 To quantify the phase locking, we first used Rayleigh's test of non-uniformity of circular data
805 (CircStat Matlab toolbox; Berens 2009). To determine whether the locking was significant for
806 individual neurons, a trial-shuffling method was used. Trial-shuffling is an efficient method for
807 obtaining a 'baseline' measure of phase locking, destroying the direct temporal relationship between
808 the two signals, while preserving their individual properties such as rhythmicity. 1000 repetitions of
809 the phase-locking analysis (Rayleigh's test) was done while randomly combining beta phases and
810 spike times from different trials. If the original data yielded a larger z-statistic value from the
811 Rayleigh's test than 950/1000 (equivalent to $p<0.05$) of the trial-shuffled controls, the phase-locking
812 of the neuron was considered significant.
813

LM and cross-correlation analysis to link the two beta bands to behavioral regressors

Dataset preprocessing

Given the similarity in the behavioral and neuronal data from the two animals up to this point, for all subsequent analyses we combined LFPs for both monkeys, while splitting low and high band dominant sites. We furthermore continued the analyses using the single-trial instantaneous beta amplitude. For each LFP site, we first bandpass filtered the signal to extract the dominant beta band, either 16+/-4Hz for low dominant sites or 26+/-5Hz for high dominant sites, using 8th order Butterworth filters. We next calculated the instantaneous amplitude (envelope) of the beta filtered LFP time series by constructing the analytic signal using the Hilbert transform. The LFP was then cut in trials, before normalizing the beta amplitude by subtracting the grand mean amplitude and dividing by the grand amplitude standard deviation. After normalization, individual trials for all LFP sites with the same beta band dominance were lumped to construct large matrices (trials x time) for each of the two beta bands, combining data from the two monkeys (Fig. 4B).

The eye signals (position and velocity) were upsampled to 1KHz, to have the same temporal resolution as the LFP and hand signals. The eye velocity was upsampled using a linear interpolation whereas the position of the gaze in the different clusters of the work area was upsampled using the nearest neighbor interpolation.

Bayesian Index Criterion

To evaluate the relation between complementary continuous and categorical variables with the LFP signal, we performed a Linear Model (LM) analysis. The LFP from both low and high beta bands were the variables to explain. The regressors considered to explain the data were 7 : color conditions (3 levels), movement direction (correct target location, 4 levels), reaction time (normalized with a z-score inside each recording session), trial number (relative position of the trial within the recording session), hand velocity (cm/s), eye velocity (cm/s) and the gaze position of the animal (inside vs outside the work area, 2 levels) and all 2-by-2 interactions. More complex interactions were excluded from the model to simplify the interpretation of the results and reduce the number of potential

regressors. We considered a total of 6800 ms, from -1200ms to 5600ms from the SEL for the analysis. All the neuronal and behavioral data were then binned in 10ms non-overlapping windows. In each bin we applied a total of 247 models (all combinations of 1 to 7 regressors including or not their 2-by-2 interactions) and compared them using a Bayesian Index Criterion (BIC). The BIC is sensitive to the number of trials considered in each model fitting. Consequently, we applied the same selection for each model, removing from all bins the trials in which the eye or the hand signals were missing, and furthermore removing trials in individual bins if the eye signal was saturated because of an eyeblink or an extreme eye position outside the dynamic range of the eye camera. We then examined the presence or not of a regressor and or interactions in the winning model in each of the 680 bins. This first analysis allowed us to target the regressors explaining the most trial-by-trial variability of high and low beta amplitude (Fig. 4A).

Linear Model Analysis

Based on the BIC analysis, 6 regressors, without interactions, were selected. Movement direction and all the possible pair-wise interactions were discarded because they were rarely represented in the regressors explaining the most the beta. The trial selection was different for each selected regressor, based on available trials for each regressor. All trials could be used color condition, RT and time-on-task (trial number) regressors. Good quality of the hand signal was necessary for the hand velocity regressor. Good quality of the eye signal was necessary for the gaze position and eye velocity regressors. For both eye gaze and velocity In both cases the eyeblinks were considered as outliers and the corresponding single-trial bins with an eyeblink were removed for the model fitting. For the analysis of the eye velocity, the remaining bins with out-of-range signal saturation in which the eye signal was saturated were furthermore removed. The different number of trials available considered for each been and each regressor prompted led us to consider each regressor separately. For each bin, each regressor and each beta band, we applied a regression model (*fitlm*) to describe the relationship between beta amplitude and the 6 different predictors. Considering that some variables

were categorical, we applied an ANOVA to the model objects to test the significance of the categorical variables. P-values <0.01 were considered significant.

Covariances matrix between hand velocity and low beta amplitude

An analysis equivalent to the joint peristimulus time histogram representation of the covariance between two neurons (Aertsen et al. 1989, Nougaret and Genovesio 2018) was applied using the hand velocity and the low beta amplitude as input signals. The mean of the variance of the trial-by-trial cross product was computed using the FieldTrip toolbox (Oostenveld et al. 2011) to obtain the *raw* covariance matrix. Then, the trials were shuffled for one variable and the same matrix was obtained, the *shuffled* covariance matrix. This procedure was performed 100 times to obtain a distribution of 100 *shuffled* covariance matrices. The corrected covariance matrix was obtained by subtracting the mean of the 100 *shuffled* covariance matrices from the *raw* covariance matrix and to divide this *subtracted* matrix by the square root of the cross product of the time-dependent variance of the *raw* matrix. The scale of the *subtracted* covariance matrix is thereby bounded between -1 and 1 and named correlation coefficients. At each point in the covariance matrix, a correlation was considered significant if the value in that point in of the *raw* covariance matrix (before correction) was always superior or always inferior to the 100 values from the *shuffle* matrices in the same point (Fig. 5A left). The data along the diagonal of the subtracted covariance matrix was averaged to obtain a lag versus correlation coefficient plot (Fig. 5A right). The lag with the largest negative value (anticorrelation) was determined in the trial period prior to and after valid SC onset.

Decoding task condition with beta amplitude

We built two classifiers using high and low beta bands separately. For each, the features were extracted from the temporal evolution of beta amplitude in single trials. We calculated the average beta amplitude in 50ms non-overlapping time bins from touch to GO in each trial. A random forest estimator was trained with the default parameters from the scikit-learn library (Pedregosa et al. 2011). Correct trials were split in a 60-40% ratio between train and test set, respectively. The model

predicted the color of SEL based on the time courses of beta amplitude. To ensure stability of the method, we repeated the procedure using 20 different data splits, always with class balance in the train set. The average performance for each of the classes was computed by averaging across repetitions. After training the classifier in the correct trials, the same model was used to predict incorrect trials. In this case, we predicted either the color of the attended (distractor) SC, or the color of SEL; i.e., the SC the monkey actually used, or the SC the monkey should have used. The chance level was calculated by shuffling the labels in 100 train-test splits of the data for both high and low beta classifiers. All the accuracy values estimated in the different shuffle test-sets were below 0.37, which we set as the overall chance level for the results.

FUNDING

This work was supported by funding from the H2020-MSCA-ITN grant *In2PrimateBrains* (#956669) and the FLAG-ERA grant *PrimCorNet*, by ANR (ANR-19-HBPR-0005) to BEK.

ACKNOWLEDGEMENTS

The authors declare no competing financial interests. The authors wish to thank Joel Baurberg, Xavier Degiovanni and Luc Renaud for technical assistance, Sébastien Barniaud, Laurence Boes, Frédéric Charlin and Marc Martin for animal care.

REFERENCES

Androulidakis, AG, Doyle, LM, Gilbertson, TP, Brown, P. (2006) Corrective movements in response to displacements in visual feedback are more effective during periods of 13–35 Hz oscillatory synchrony in the human corticospinal system. Eur J Neurosci 24: 3299-3304.

Aertsen AM, Gerstein GL, Habib MK, Palm G (1989) Dynamics of neuronal firing correlation: modulation of 'effective connectivity'. J Neurophysiol 61, 900–917.

Asanuma H, Rosén I. (1972) Topographical organization of cortical efferent zones projecting to distal forelimb muscles in the monkey. Exp Brain Res 14:243–256

Baker SN, Kilner JM, Pinches EM, Lemon RN (1999) The role of synchrony and oscillation in the motor output. Exp Brain Res 128:109–117.

Barone J, Rossiter HE (2021) Understanding the Role of Sensorimotor Beta Oscillations. Front Syst Neurosci 15:655886.

Berens P (2009) CircStat: A Matlab Toolbox for Circular Statistics. J Stat Soft 31:1-21.

Brown P (2000) Cortical drives to human muscle: the Piper and related rhythms. Progress in neurobiology 60(1):97-108.

Buschman TJ, Denovellis EL, Diogo C, Bullock D, Miller EK (2012) Synchronous oscillatory neural ensembles for rules in the prefrontal cortex. Neuron 76:838–846.

Buschman TJ, Miller EK (2007) Top-down versus bottom-up control of attention in the prefrontal and posterior parietal cortices. Science 315:1860-1862.

Chandrasekaran C, Bray IE, Shenoy KV (2019) Frequency shifts and depth dependence of premotor beta band activity during perceptual decision making. J Neurosci 39:1420 –1435.

Chota S, VanRullen R, Gulbinaite R (2023) Random Tactile Noise Stimulation Reveals Beta-Rhythmic Impulse Response Function of the Somatosensory System. J Neurosci 16:JN-RM-1758-22.

Confais J, Kilavik BE, Ponce-Alvarez A, Riehle A (2012) On the anticipatory precue activity in motor cortex. J Neurosci 32:15359–15368.

Confais J, Malfait N, Brochier T, Riehle A, Kilavik BE (2020) Is there an intrinsic relationship between LFP beta oscillation amplitude and firing rate of individual neurons in macaque motor cortex? Cerebral Cortex Communications 1(1):tgaa017.

Conway BA, et al. (1995) Synchronization between motor cortex and spinal motoneuronal pool during the performance of a maintained motor task in man. J Physiol 489:917-924.

Courtemanche R, Fujii N, Graybiel AM (2003) Synchronous, focally modulated beta-band oscillations characterize local field potential activity in the striatum of awake behaving monkeys. J Neurosci 23:11741-11752.

Courtemanche R, Lamarre Y (2005) Local field potential oscillations in primate cerebellar cortex: synchronization with cerebral cortex during active and passive expectancy. J Neurophysiol 93:2039-2052.

Crameri, F (2021) Scientific colour maps (7.0.1). Zenodo. https://doi.org/10.5281/zenodo.5501399

de Haan MJ, Brochier T, Grün S, Riehle A, Barthélemy FV (2018) Real-time visuomotor behavior and electrophysiology recording setup for use with humans and monkeys. J Neurophysiol 120:539-52

Donoghue JP, Sanes JN, Hatsopoulos NG, Gaál G (1998) Neural discharge and local field potential oscillations in primate motor cortex during voluntary movements. J Neurophysiol 79(1):159-173.

Donoghue T, et al. (2020). Parameterizing neural power spectra into periodic and aperiodic components. Nat Neurosci 23(12):1655-1665.

951 Echeverria-Altuna I, et al. (2022) Transient beta activity and cortico-muscular connectivity during
952 sustained motor behaviour. Prog Neurobiol 214:102281.

953 Engel AK, Fries P (2010) Beta-band oscillations – signalling the status quo?
954 Curr Opin Neurobiol 20:156-165.

955 Feingold J, Gibson DJ, DePasquale B, Graybiel AM (2015) Bursts of beta oscillation differentiate
956 postperformance activity in the striatum and motor cortex of monkeys performing movement tasks.
957 Proc Natl Acad Sci U S A 112(44):13687-13692.

958 Fujioka T, Trainor LJ, Large EW, Ross B (2012) Internalized timing of isochronous sounds is
959 represented in neuromagnetic Beta oscillations. J Neurosci 32:1791–1802.

960 Haegens S, et al. (2011) Beta Oscillations in the monkey sensorimotor network reflect
961 somatosensory decision making. Proc Natl Acad Sci USA 108:10708-10713.

962 Hafed ZM, Clark JJ (2002) Microsaccades as an overt measure of covert attention shifts. Vision Res
963 42(22):2533-2545.

964 Jasper H, Penfield W (1949) Electrocorticograms in man: effect of voluntary movement upon the
965 electrical activity of the precentral gyrus. Arch Psychiatr Zeitschr Neurol 83:163-174.

966 Jenkinson N, Brown P (2011) New insights into the relationship between dopamine, beta
967 oscillations and motor function. Trends Neurosci 34:611–618.

968 Jensen O, et al. (2005) On the human sensorimotor-cortex beta rhythm: sources and modeling.
969 NeuroImage 26:347-355.

970 Kilavik BE, Confais J, Ponce-Alvarez A, Diesmann M, Riehle A (2010) Evoked potentials in motor
971 cortical LFPs reflect task timing and behavioral performance. J Neurophysiol 104:2338-2351.

972 Kilavik BE, Confais J, Riehle A (2014) Signs of timing in motor cortex during movement preparation
973 and cue anticipation. Adv Exp Med Biol. 829:121-142.

974 Kilavik BE, Confais J, Riehle A (2014) Signs of timing in motor cortex during movement preparation
975 and cue anticipation. Neurobiology of Interval Timing 121-142.

976 Kilavik BE, Ponce-Alvarez A, Trachel R, Confais J, Takerkart S, Riehle A (2012) Context-related
977 frequency modulations. Cereb Cortex 22(9):2148-2159.

978 Kilavik BE, Zaepffel M, Brovelli A, MacKay WA, Riehle A (2013) The ups and downs of beta
979 oscillations in sensorimotor cortex. Exp Neurol 245:15-26.

980 Kühn AA, et al. (2009) Frequency-specific effects of stimulation of the subthalamic area in treated
981 Parkinson's disease patients. Neuroreport 20(11):975-8.

982 Lalo E, et al. (2007) Phasic increases in cortical beta activity are associated with alterations in
983 sensory processing in the human. Exp Brain Res 177(1):137-145.

984 López-Azcárate J, et al. (2010) Coupling between beta and high-frequency activity in the human
985 subthalamic nucleus may be a pathophysiological mechanism in Parkinson's disease. J Neurosci
986 30:6667– 6677.

987 Lundqvist M, Bastos AM, Miller EK (2020) Preservation and Changes in Oscillatory Dynamics
988 across the Cortical Hierarchy. J Cogn Neurosci 32(10):2024-2035.

989 Lundqvist M, et al. (2016) Gamma and Beta Bursts Underlie Working Memory. Neuron 90:152-
990 164.

991 Mahjoory K, Schoffelen JM, Keitel A, Gross J (2020) The frequency gradient of human resting-state
992 brain oscillations follows cortical hierarchies. Elife 9:e53715.

Murthy VN, Fetz EE (1996) Synchronization of neurons during local field potential oscillations in sensorimotor cortex of awake monkeys. J Neurophysiol 76:3968-3982.

Murthy VN, Fetz EE. 1992. Coherent 25- to 35-Hz oscillations in the sensorimotor cortex of behaving monkeys. Proc Natl Acad Sci USA 89:5670-5674.

Musall S, Kaufman MT, Juavinett AL, Gluf S, Churchland AK (2019) Single-trial neural dynamics are dominated by richly varied movements. Nat Neurosci 22(10):1677-1686.

Neumann WJ, et al. (2016) Subthalamic synchronized oscillatory activity correlates with motor impairment in patients with Parkinson's disease. Mov Disord 31(11):1748-1751.

Nougaret S, Genovesio A (2018) Learning the meaning of new stimuli increases the cross-correlated activity of prefrontal neurons. *Sci Rep.*8, 11680.

Oostenveld R, Fries P, Maris E, Schoffelen J (2011) FieldTrip: Open Source Software for Advanced Analysis of MEG, EEG, and Invasive Electrophysiological Data. Comput. Intell. Neurosci. 1–9.

Ortega J, Plaska CR, Gomes BA, Ellmore TM (2022) Spontaneous Eye Blink Rate During the Working Memory Delay Period Predicts Task Accuracy. Front Psychol 13:788231.

Pastötter B, Berchtold F, Bäuml KHT (2011) Oscillatory correlates of controlled speed-accuracy tradeoff in a response-conflict task. Hum Brain Mapp 33(8):1834-1849.

Pedregosa et al. 2011. Scikit-learn: Machine Learning in Python, JMLR 12: 2825-30.

Peles O, et al. (2020) Microstimulation Differentially Modulates Beta Oscillations and Affects Behavior. Cell Rep 30(8):2555-2566.e3.

Perfetti B, et al. (2011) Temporal evolution of oscillatory activity predicts performance in a choice-reaction time reaching task. J Neurophysiol 105:18-27.

Ponce-Alvarez A, Kilavik BE, Riehle A. (2010) Comparison of local measures of spike time irregularity and relating variability to firing rate in motor cortical neurons. J Comput Neurosci 29:351-365.

Priori A, et al. (2004) Rhythm-specific pharmacological modulation of subthalamic activity in Parkinson's disease. Exp Neurol 189(2):369-79.

Rassi E, et al. (2022) Distinct beta frequencies reflect categorical decisions. bioRxiv 2022.10. 17.512497.

Rosanova M, et al (2009) Natural frequencies of human corticothalamic circuits. J Neurosci 29(24):7679-85.

Rougeul A, Bouyer JJ, Dedet L, Debray O (1979) Fast somato-parietal rhythms during combined focal attention and immobility in baboon and squirrel monkey. Electroencephalogr Clin Neurophysiol 46:310-319.

Rubino D, Robbins KA, Hatsopoulos NG (2006) Propagating waves mediate information transfer in the motor cortex. Nat Neurosci 9(12):1549-57.

Haegens S, Vergara J, Rossi-Pool R, Lemus L, Romo R (2017) Beta oscillations reflect supramodal information during perceptual judgment. PNAS 114:13810-13815.

Saleh M, Reimer J, Penn R, Ojakangas CL, Hatsopoulos NG (2010) Fast and slow oscillations in human primary motor cortex predict oncoming behaviorally relevant cues. Neuron 65:461-471.

Salmelin R, Hämäläinen M, Kajola M, Hari R (1995) Functional segregation of movement-related rhythmic activity in the human brain. Neuroimage 2(4):237-243.

Sanes JN, Donoghue JP (1993) Oscillations in local field potentials of the primate motor cortex during voluntary movement. Proc Natl Acad Sci USA 90:4470-4474.

Schmidt R, et al. (2019) Beta Oscillations in Working Memory, Executive Control of Movement and Thought, and Sensorimotor Function. J Neurosci 39(42):8231-8238.

Spitzer B, Haegens S (2017) Beyond the status quo: a role for beta oscillations in endogenous content (re)activation. eNeuro 4(4):ENEURO.0170-17.2017.

Stoll FM, et al (2016). The Effects of Cognitive Control and Time on Frontal Beta Oscillations. Cereb Cortex 26(4):1715-1732.

Sun H, et al (2019). Modulation of Beta Oscillations for Implicit Motor Timing in Primate Sensorimotor Cortex during Movement Preparation. Neurosci Bull 35(5):826-840.

Tremblay S, Testard C, DiTullio RW, Inchauspé J, Petrides M (2023) Neural cognitive signals during spontaneous movements in the macaque. Nat Neurosci 26(2):295-305.

Van Ede F, de Lange F, Jensen O, Maris E (2011) Orienting attention to an upcoming tactile event involves a spatially and temporally specific modulation of sensorimotor alpha- and beta-band oscillations. J Neurosci 31:2016–2024.

Van Ede F, Jensen O, Maris E (2010) Tactile expectation modulates pre-stimulus beta-band oscillations in human sensorimotor cortex. NeuroImage 51:867–876.

Vezoli J, et al (2021). Brain rhythms define distinct interaction networks with differential dependence on anatomy. Neuron 109(23):3862-3878.e5.

Wiener M, Parikh A, Krakow A, Coslett HB (2018) An Intrinsic Role of Beta Oscillations in Memory for Time Estimation. Sci Rep 8(1):7992.

Witham CL, Baker SN (2007) Network oscillations and intrinsic spiking rhythmicity do not covary in monkey sensorimotor areas. J Physiol 580(Pt.3):801-14.

Witham CL, Riddle CN, Baker MR, Baker SN (2011) Contributions of descending and ascending pathways to corticomuscular coherence in humans. J Physiol 589:3789-3800.

Witham CL, Wang M, Baker SN (2007) Cells in somatosensory areas show synchrony with beta oscillations in monkey motor cortex. Eur J Neurosci 26:2677-86.

Witham CL, Wang M, Baker SN (2010) Corticomuscular coherence between motor cortex, somatosensory areas and forearm muscles in the monkey. Front Syst Neurosci 4:38.

Zanos S, Rembado I, Chen D, Fetz EE (2018) Phase-Locked Stimulation during Cortical Beta Oscillations Produces Bidirectional Synaptic Plasticity in Awake Monkeys. Curr Biol. 28:2515-2526.e4.

Zhang Y, Wang X, Bressler SL, Chen Y, DingM (2008) Prestimulus cortical activity is correlated with speed of visuomotor processing. J Cogn Neurosci 20:1915–1925.

1067 **FIGURE LEGENDS**

1068

1069 **Figure 1. Experimental setup and task, spontaneous hand and eye movements.**

1070 A. The monkeys were seated in a primate chair, and performed center-out arm reaching
1071 responses with a manipulandum in the horizontal plane for water or juice reward, with the visual
1072 scene displayed on a vertical monitor. Eye position was recorded using an infrared camera.

1073 B. The monkeys performed a visuomotor rule-based and predictive cue-selection task. The trial
1074 started when the monkey moved the hand cursor to the central fixation spot (touch). Next, a
1075 selection cue (SEL) indicated the color to attend in that trial. Thereafter three spatial cues (SC) were
1076 presented in sequence in fixed order (blue SC1 – green SC2 – pink SC3), each in one of the four
1077 possible peripheral target positions. A directionally non-informative GO signal indicated to the
1078 monkey to initiate the center-out reaching movement to the memorized valid target location. Each
1079 delay lasted 1s and each visual cue lasted 300ms.

1080 C. Average hand velocity across all trials in all behavioral sessions in each monkey, zoomed in to
1081 the micro-movements performed during the trial between central touch and the GO signal. In this
1082 and subsequent figures, the blue, green and pink lines reflect data split according to the color
1083 condition. Vertical dotted lines reflect onset/offset of visual task events.

1084 D. Average eye velocity in each monkey across all trials in all behavioral sessions with eye
1085 movement recordings. Same conventions as in C.

1086 E. Gaze position in monkey T, across all behavioral sessions with eye movement recordings, in
1087 blue (upper), green (middle) and pink (bottom) color conditions. Each plot show the total proportion
1088 of trials with eye gaze on the Target SC (cyan), on one of the distractor SC (orange), on the central
1089 fixation spot (yellow), between different visual items on the monitor (purple), outside the work area
1090 (monitor; gray) or eyeblinks (black). Vertical lines reflect onset/offset of visual task events.

1091 F. Gaze position in Monkey M. Same conventions as in E.

1092

Figure 2. Example LFP sites and grand average spectrogram.

A-C. Spectrograms of three simultaneously recorded LFP sites from monkey T, including all correct trials in one session, separated for the blue (top), green (middle) and pink (bottom) color conditions. The locations of the three example LFP sites are marked with stars in Figure 3C, with site 1 the more anterior and site 3 the more posterior. Frequency is on the vertical axis and task events are indicated along the horizontal axis. Warmer colors indicate increased power (a.u.).

D. Single trial examples of LFPs filtered broadly around the beta frequency range (8-45Hz), for LFP site 1. Five trials per color condition are shown.

E. Grand average spectrograms for each monkey, including normalized individual trials for all LFP sites in each monkey.

F. As in D, but for LFP site 3.

Figure 3. Concurrent low and high beta band rhythms in motor cortex.

A. Average normalized power spectra in the pre-SC1 period across all trials for all sites in each monkey. The curves reflect the mean power ±SEM across LFP sites. The power spectral density for each LFP site was normalized to the mean power between 10 and 40 Hz before averaging across all trials in all sites. Overlain are distributions of single-trial peak frequency (frequency with maximal power) between 10-40Hz in the same period.

B. Distribution of the beta band dominance index for all LFP sites for each monkey, based on the pre-SC1 period. Positive indices reflect low band (13-19Hz) dominance and negative indices reflect high band (23-29Hz) dominance. Light gray bars include all sites, and black bars sites with significantly different power in the low and high beta frequency ranges (paired t-test, $p<0.05$).

C. Beta band dominance index distribution across the cortical surface. The indices for both monkeys are plotted on top of the cortical surface reconstruction of monkey T (anterior towards the left, and medial towards the top). Blue sites reflect high band dominance, and yellow sites reflect low

band dominance. The three sites from anterior to posterior marked with red asterixes (*) reflect the example sites shown in Fig. 2. CS central sulcus; AS arcuate sulcus; PCD pre-central dimple.

D. Average spectrograms for all high (left) and low (right) beta band dominant LFP sites for each monkey.

Figure 4. Main regressors explaining the High and Low beta variance.

A. Representation along the trial of the presence of the regressor in the winning model after the application of a Bayesian Index Criterion (BIC) for the comparison of all possible models and their 2-by-2 interactions, for the high beta (left) and the low beta (right). Each row represents a regressor, the last row represents all possible interactions.

B. Bottom. Representation of the average normalized high (left ; 21-29Hz) and low (right ; 12-20Hz) beta amplitude (+/-SEM) along the trial, separated by the 3 color conditions. Top. Each horizontal graph represents the significativity of the trial-by-trial modulation in beta amplitude by a defined variable. The variables are, from bottom to top, color condition, eye velocity and hand velocity (the two latter split into three graphs for the three color conditions). The significativity is represented as a color gradient, white means non-significant, colored means significant, split in significant positive correlations top and negative correlations bottom. The gradient of brightness in the color is a gradual representation of the p-value from 0.01 (lightest color) to 1e-08 (darkest color).

Figure 5. Correlations of low beta amplitude with hand velocity and RT.

A. Left. Equivalent of a joint peristimulus time histogram applied to the hand velocity and the low beta amplitude along the trial. Each point of the matrix represents the corrected trial-by-trial cross product of the two variables. The analysis was performed separately for the 3 trial types, top: blue trials, middle: green trials, bottom: pink trials. Each colored matrix point was inferior (cold color) or superior (warm color) to 100 values from shuffled matrices (equivalent p-value of 0.01). The vertical and horizontal lines represent the appearance and disappearance of the valid SC for the 3 conditions.

Right. Cross correlograms. Each value of the cross correlogram represents the average of main and lagged diagonals of the matrices, separately for before (bottom) and after (top) the onset of the valid SC.

B. High beta split in two groups based on normalized RT, for each color condition. Lines above each plot indicate correlation significance (and sign) with RT. Dark colors represent the high beta for the quarter of the trials in which the monkeys were the slowest in each session (long RT). Light colors represent the high beta for the quarter of trials in which the monkeys were the fastest in each session (short RT). The representation of the significativity is the same as in Figure 4.

C. Same representation for the low beta band.

Figure 6. Correlation of high and low beta amplitude with the position of the gaze at optimal lag.

A. High beta split in two groups based on gaze position 230ms earlier for each time point, for each color condition. Lines above each plot indicate correlation significance (and sign) with preceding gaze position. Dark colors represent the high beta for the times in which the monkey's gaze was inside the working area (In). Light colors represent the high beta for the times in which the monkey's gaze was outside the working area (Out). The representation of the significativity is the same as in Figure 4.

B. Same representation for the low beta band.

Figure 7. Systematic changes in beta amplitude within sessions – Time-on-task.

A. High beta split in groups based on the time elapsed in the session, for each color condition. Lines above each plot indicate correlation significance (and sign) with the elapsed time. Dark colors represent the high beta for the first third of trials performed in each recording session. Light colors represent the high beta for the last third of trials performed in each session. The representation of the significativity is the same as in Figure 4.

B. Same representation for the low beta band.

Suppl. Fig. 1. Supplementary behavioral results.

A. Average hand velocity in one example session in monkey T, split for the three color conditions. On the left, zoomed in to the micro-movements performed during the trial between central touch and GO. To the right with velocity scale adjusted to the final center-out reaching movement after GO. Vertical dotted lines reflect onset/offset of visual task events. targ: target touch onset; rew: reward.

B. Hand velocity in a randomly selected subset of correct green trials in the same session as in A. The velocity scale is indicated on the left. Vertical dotted lines reflect onset/offset of visual task events. The two solid black vertical lines connected with a horizontal arrow reflect the epoch used to estimate X and Y offsets of micromovements in the post-cue epoch (C).

C. Hand cursor displacement caused by micro-movements across all green trials in each monkey, split for trials with targets in each of the four corners. Each dot reflects one trial, and the position reflects the relative X and Y offset 1s after the onset of SC2 (2nd vertical solid black line in B), compared to the position at SC2 onset (1st vertical solid black line in B). UR-upper right; LR-lower right; LL-lower left; UL-upper left.

D. Average hand velocity in each of the three post-SC delays, taken at 500ms after cue offset, split for color condition. Horizontal black lines on top of the bar plots denote significant differences in single-trial hand velocity between the different color conditions.

E. Deltoid EMG amplitude, recorded in the same behavioral session as shown in A-B, during the delays and split for the three color conditions (left) and aligned to movement onset and averaged for the three color conditions (right). For each color condition, we show two directions, towards and away from the animal (lower left vs. upper left targets).

Suppl. Fig 4. Beta band modulations in error trials and condition decoding with beta amplitude.

A. Average beta amplitude in high beta (left) and low beta (right) in correct and distractor error trials, split for the three color conditions from top to bottom. We only included trials in which the target selected (correct or distractor) did not coincide in space with any of the other two SC. The

thicker line in each plot represents correct trials, while the thinner lines represent the error trials in which either one or the other distractor was used.

B. Decoding performance of SEL (color condition) category in correct trials, using either high (left) or low (right) beta band amplitude. Performance is presented as proportions of the total number of trials of each category in the test set (totalling 1 for each row). The diagonal represents the true positive accuracy, and the off-diagonal values correspond to the proportions of trials of each category incorrectly assigned to another category. The chance level (0.37) is indicated on the color scale bar.

C. Decoding performance on distractor error trials, using the classifier previously trained on the correct trials. The first column for each band represents the accuracy when predicting the attended distractor (i.e. what the monkey actually did); the second column represents the accuracy when predicting the correct SEL category (i.e. what the monkey should have done). The same chance level applies to these predictions as for the decoding of correct trials.

Suppl. Fig. 5. Correlation of hand velocity with RT.

Hand velocity split in two groups based on normalized RT, for each color condition. Lines above each plot indicate correlation significance (and sign) with RT. Dark colors represent the hand velocity for the quarter of the trials in each session with longer RT. Light colors represent the hand velocity for the quarter of trials in each session with shorter RT. The representation of the significativity is the same as in Figure 4.

Suppl. Fig. 6. Correlations between beta amplitude and gaze position.

A. Top. High beta split in groups based on the monkey's position of the gaze at different time lags (Left: -230ms, Middle Oms, Right +230ms), all color conditions combined. Bottom. Same representation for the low beta band.

B. Proportion of bins in which the beta was significantly different depending on gaze position. The x-axis represents the different temporal lags that were tested. A negative lag means beta is leading gaze (i.e. a correlation between LFP at time t0 and the position of the gaze at time t0 + lag). A positive lag means beta is lagging gaze (i.e. a correlation between LFP at time t0 and the position of the gaze at time t0 – lag).

C. Low beta band split in groups of trials based on the position of the gaze at 200ms after the onset of the valid SC. Blue and orange represent the trials in which the monkeys were looking inside the working area (either on the target, or elsewhere). Yellow represents the trials in which the monkeys were looking outside the working area.

Suppl. Fig. 7. Spectral parametrization for early and late trials.

A. Spectral parametrization using FOOOF for early (left) and late (right) trials in the sessions, for each monkey separately. The black line corresponds to the original data and the red line to the model fit. The algorithm identifies the spectral peaks and their peak frequency (green). A frequency range of 5-194Hz was used for fitting the data for both monkeys.

B. Spectrum decomposition in periodic (left) and aperiodic (right) signal components, in early and late trials in the sessions, for each monkey. The frequency axis was cut at 60Hz to focus on the lower frequencies including the beta bands.

Suppl. Table 1

Summary of number of trials included for behavioral analyses, percent of distractor errors and RTs for each color condition and movement direction for each animal. UR-upper right; LR-lower right; LL-lower left; UL-upper left.

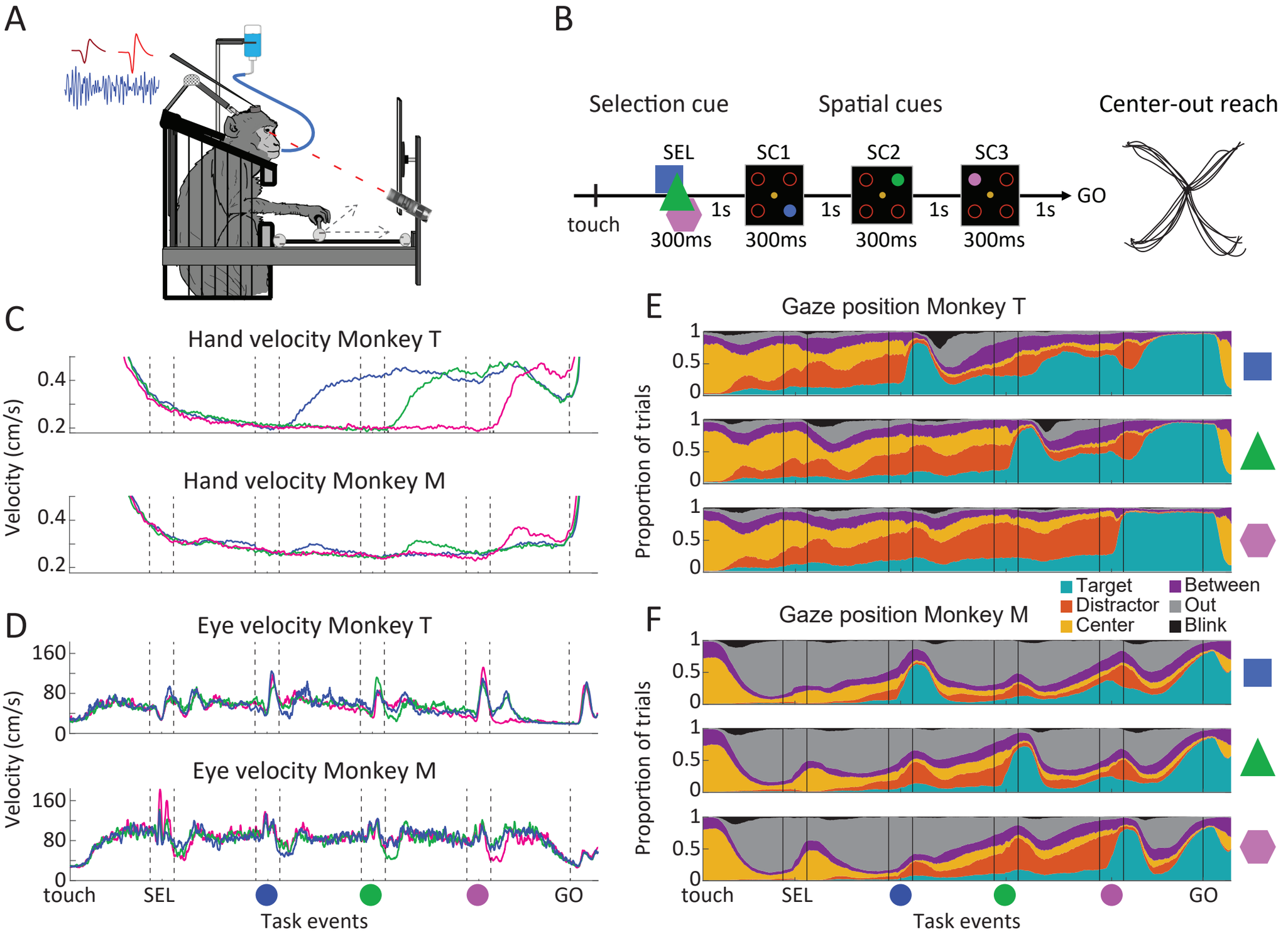

Figure 1. Experimental setup and task, spontaneous hand and eye movements.

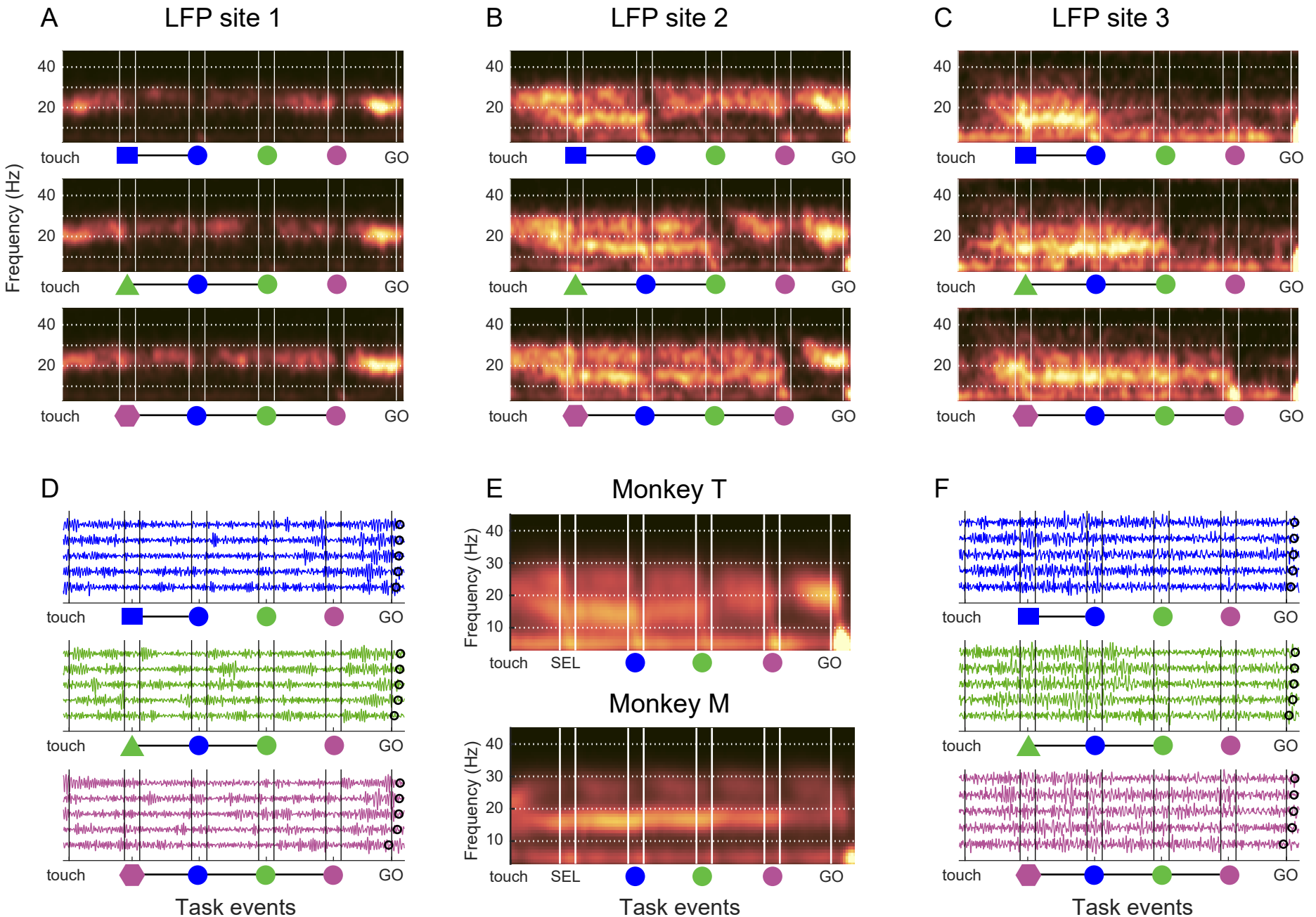

Figure 2. Example LFP sites and grand average spectrogram.

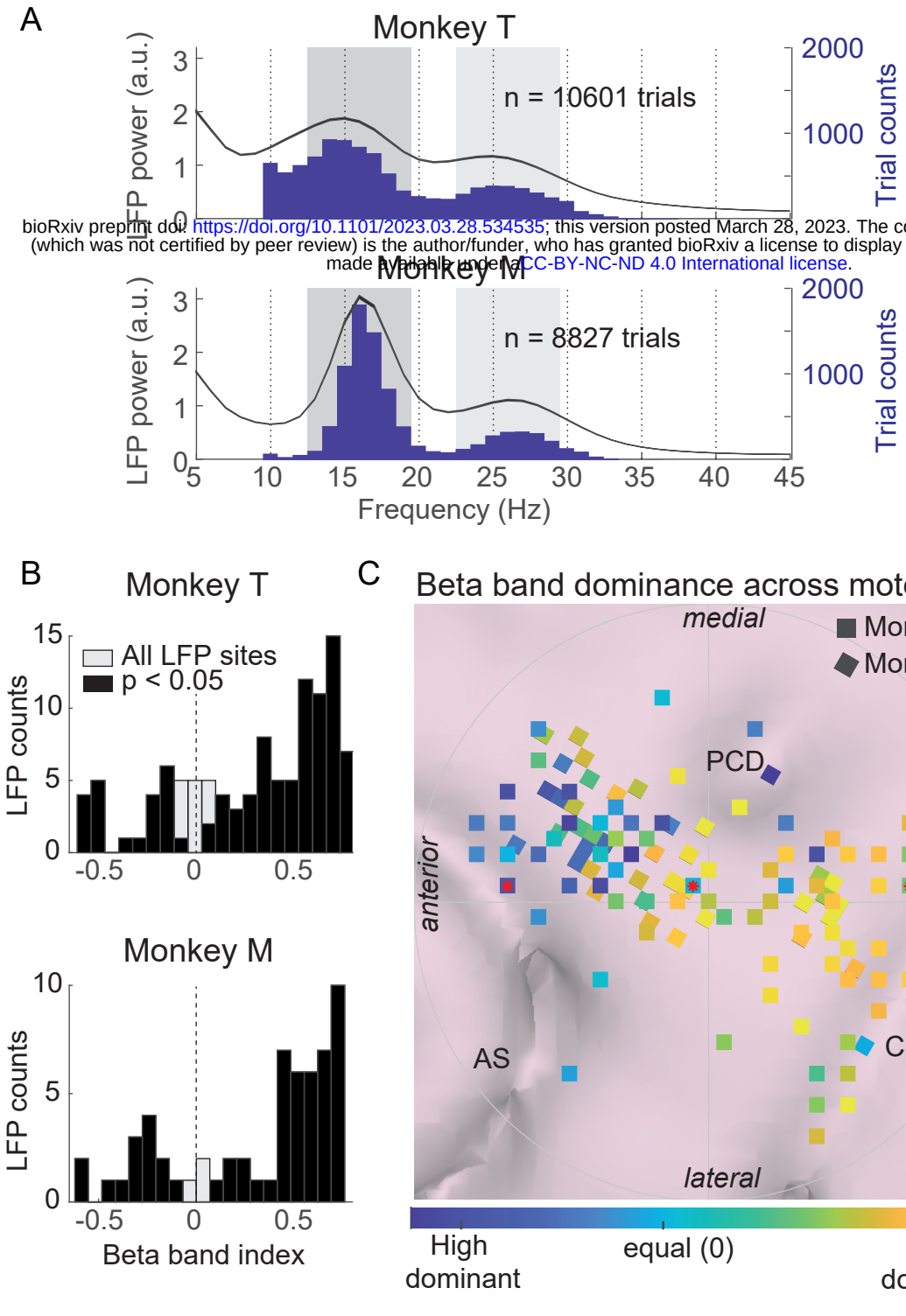

Figure 3. Concurrent low and high beta band rhythms in motor cortex.

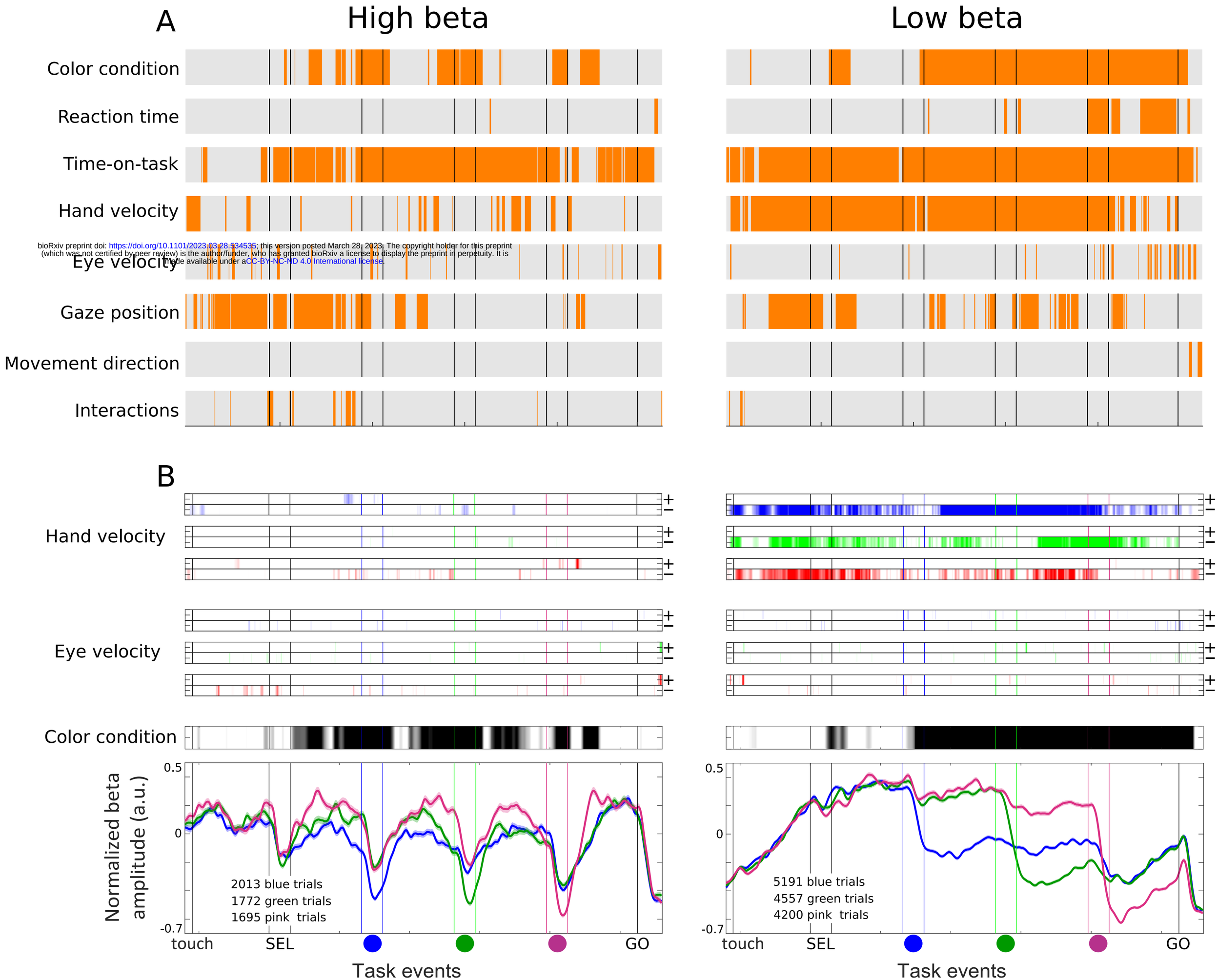

Figure 4. Main regressors explaining the High and Low beta variance.

Figure 5. Correlations of low beta amplitude with hand velocity and RT.

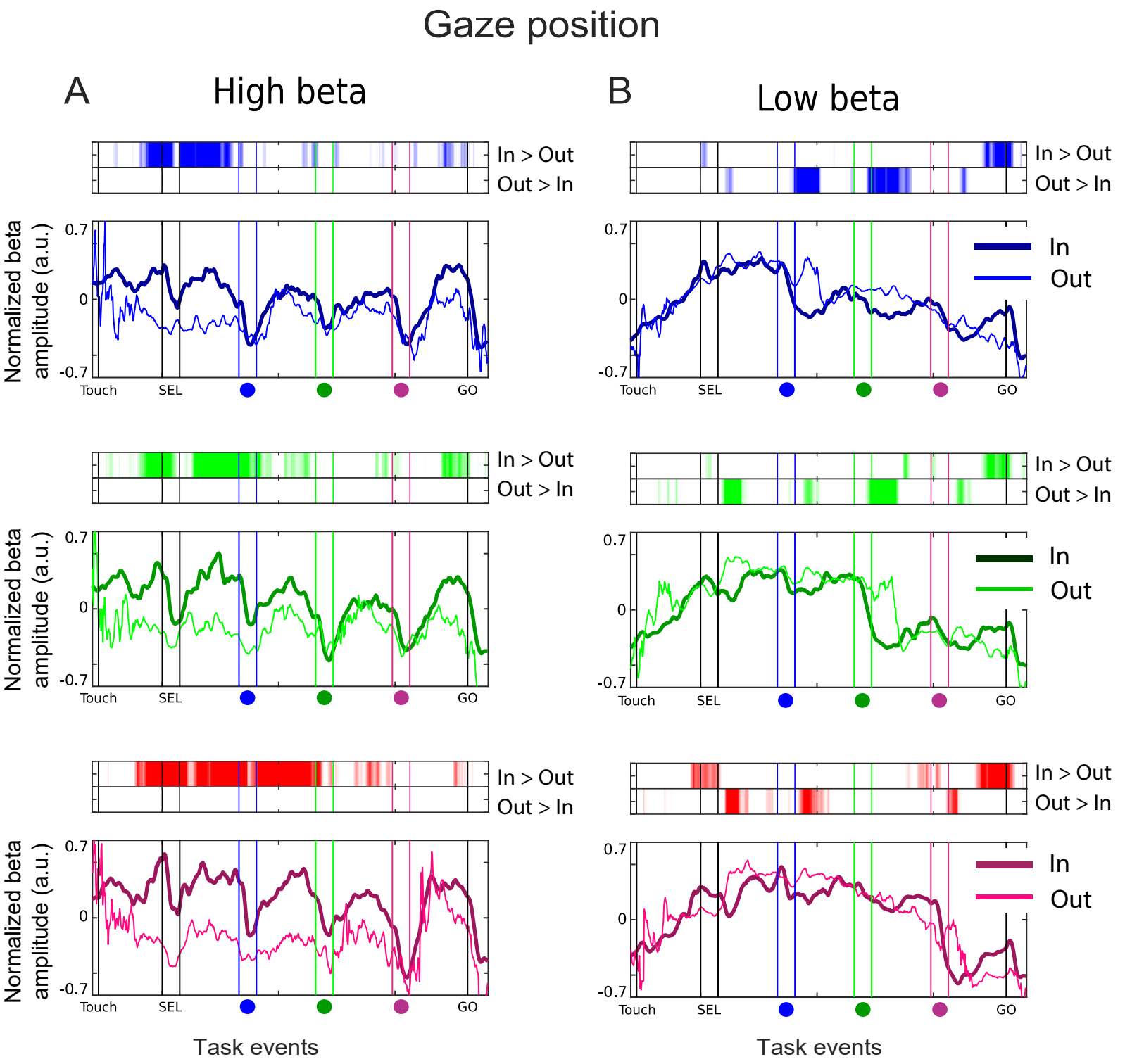

Figure 6. Correlation of high and low beta amplitude with the position of the gaze at optimal lag.

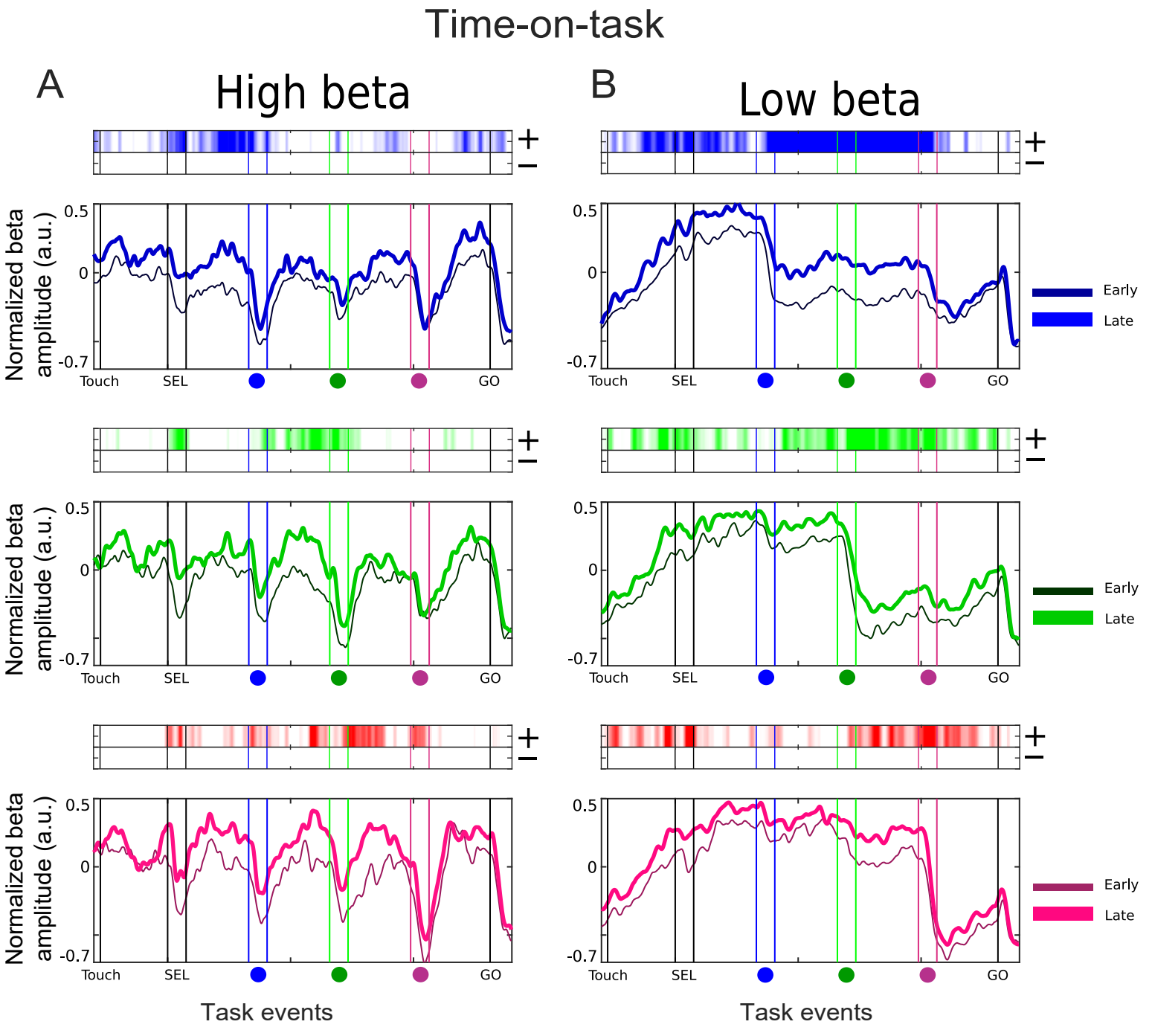

Figure 7. Systematic changes in beta amplitude within sessions – Time-on-task.

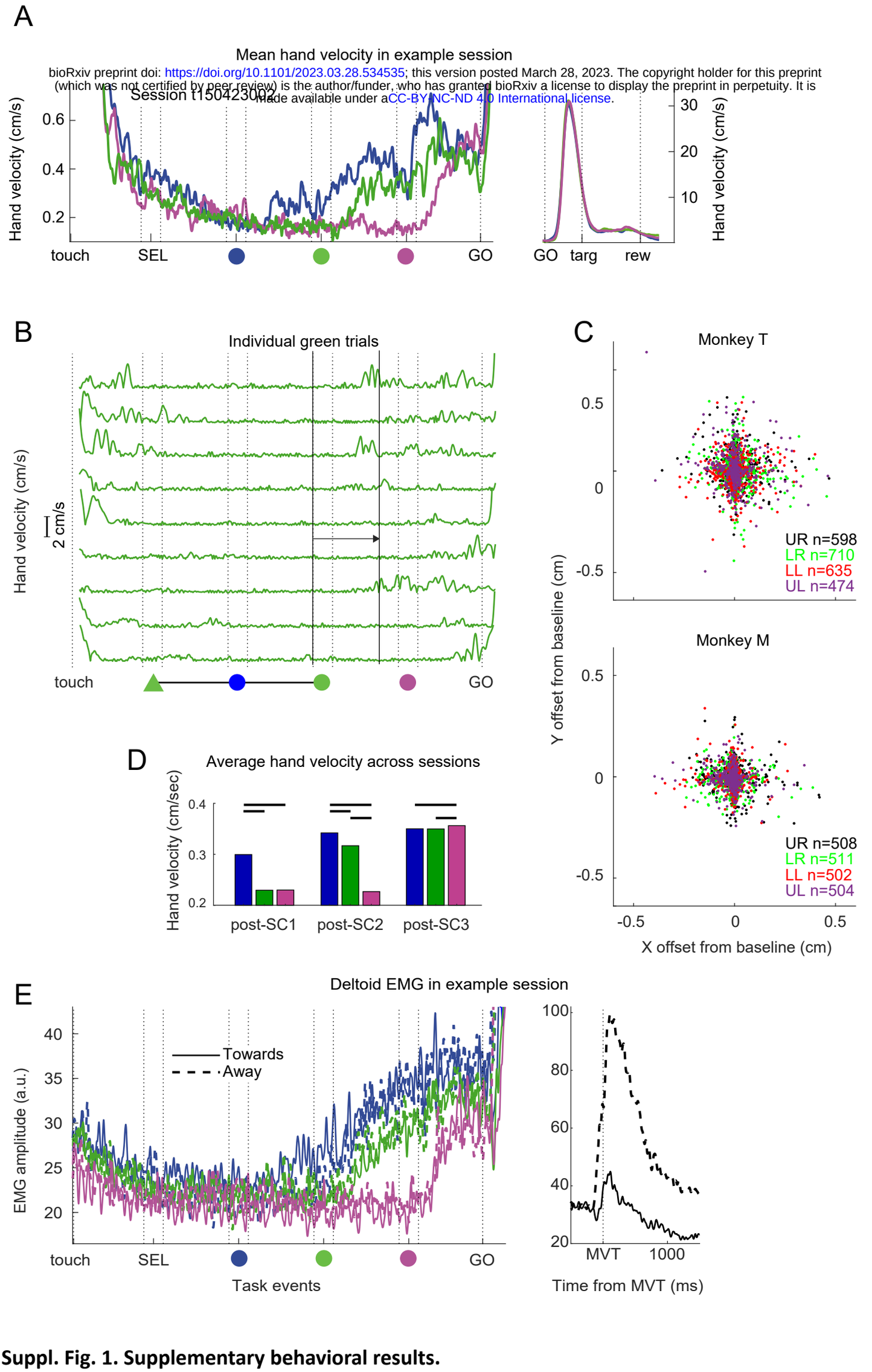

Suppl. Fig. 1. Supplementary behavioral results.

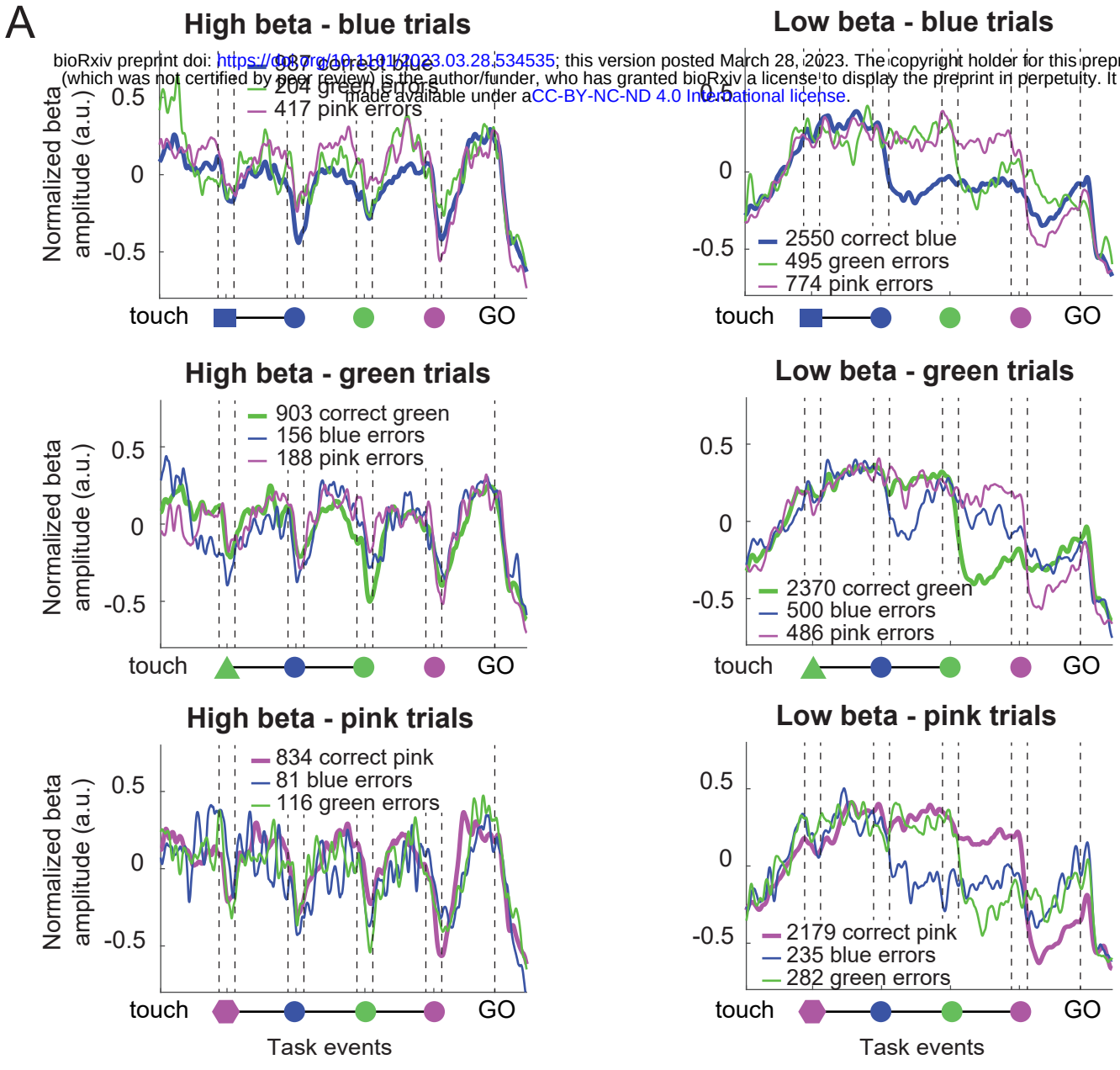

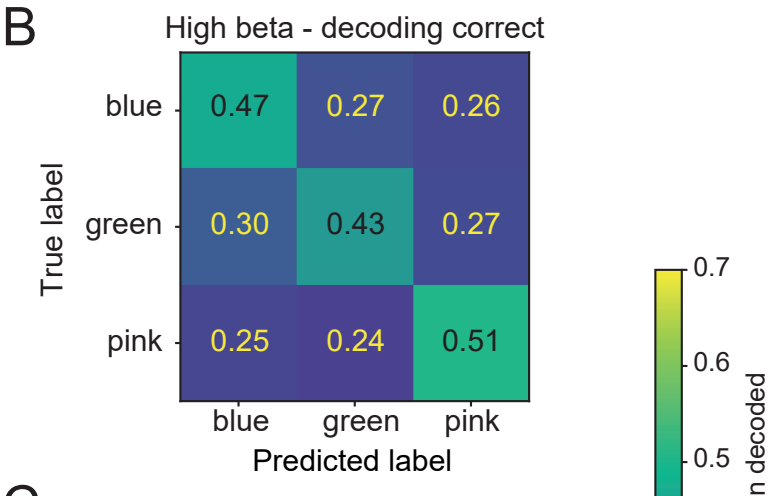

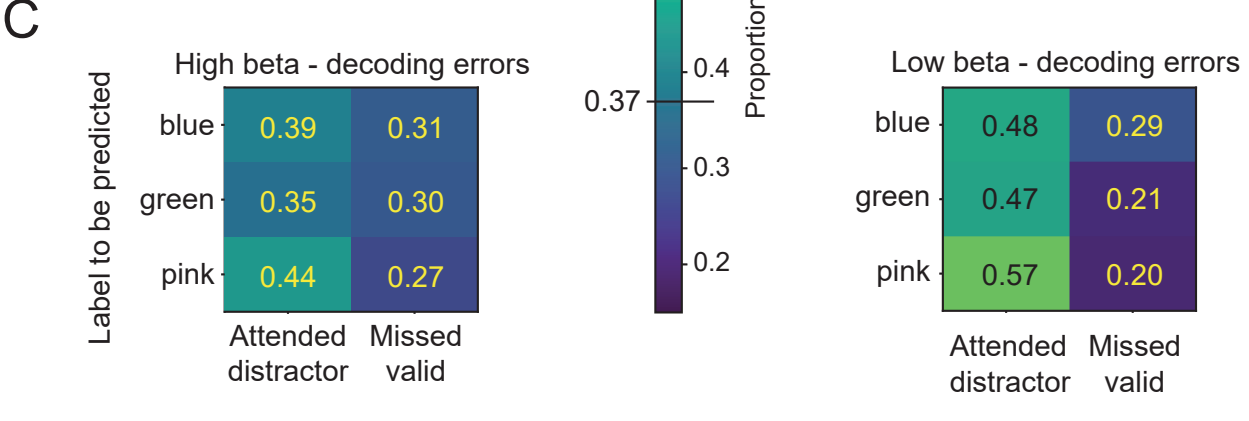

Suppl. Fig 4. Beta band modulations in error trials and condition decoding with beta amplitude.

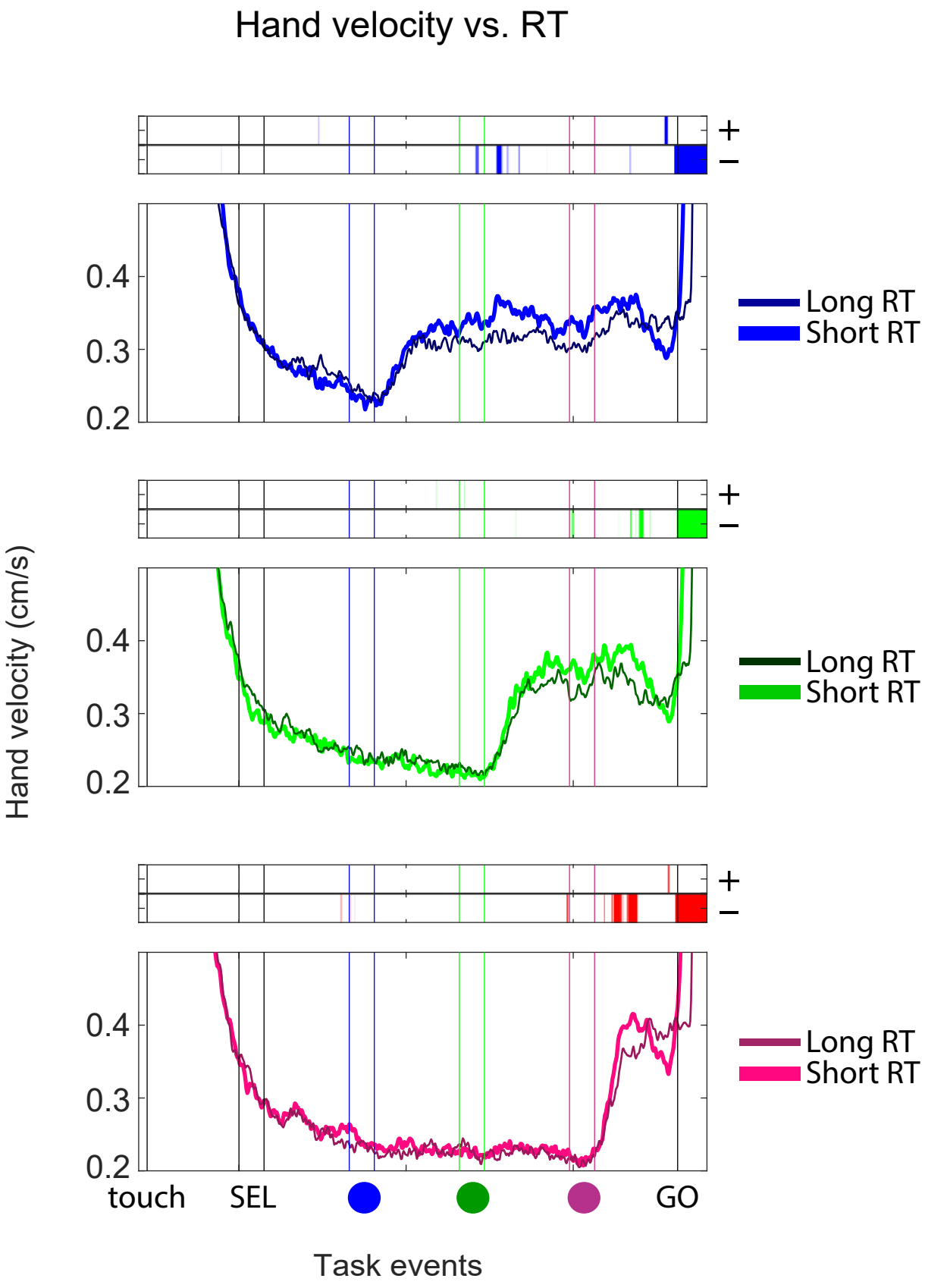

Suppl. Fig. 5 Correlation of hand velocity with RT.

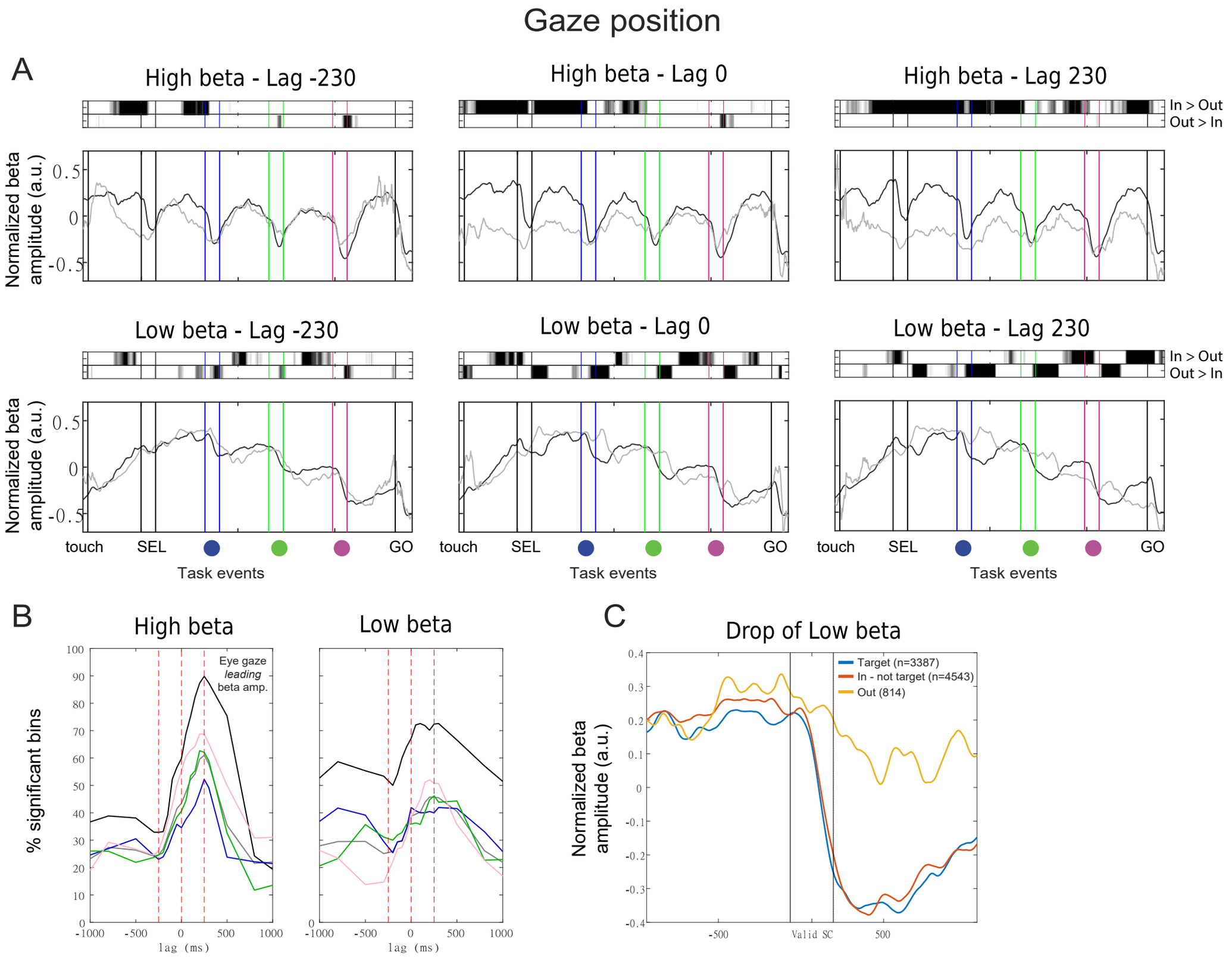

Suppl. Fig. 6. Correlations between beta amplitude and gaze position.

A

Monkey T

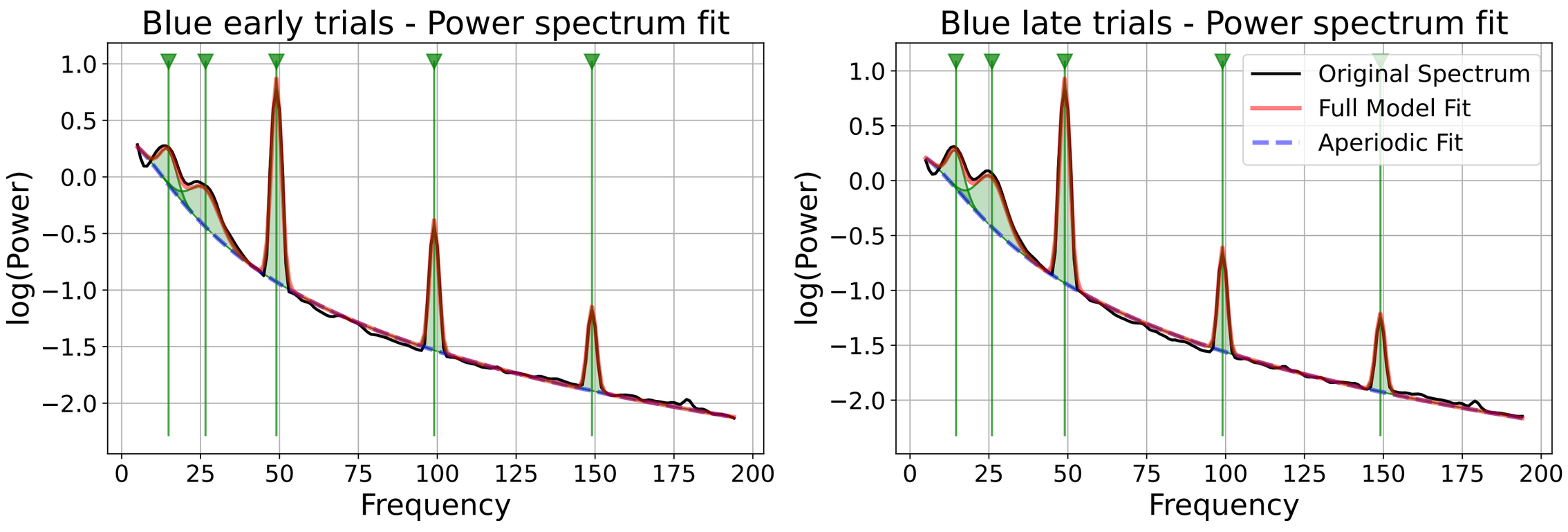

Monkey M

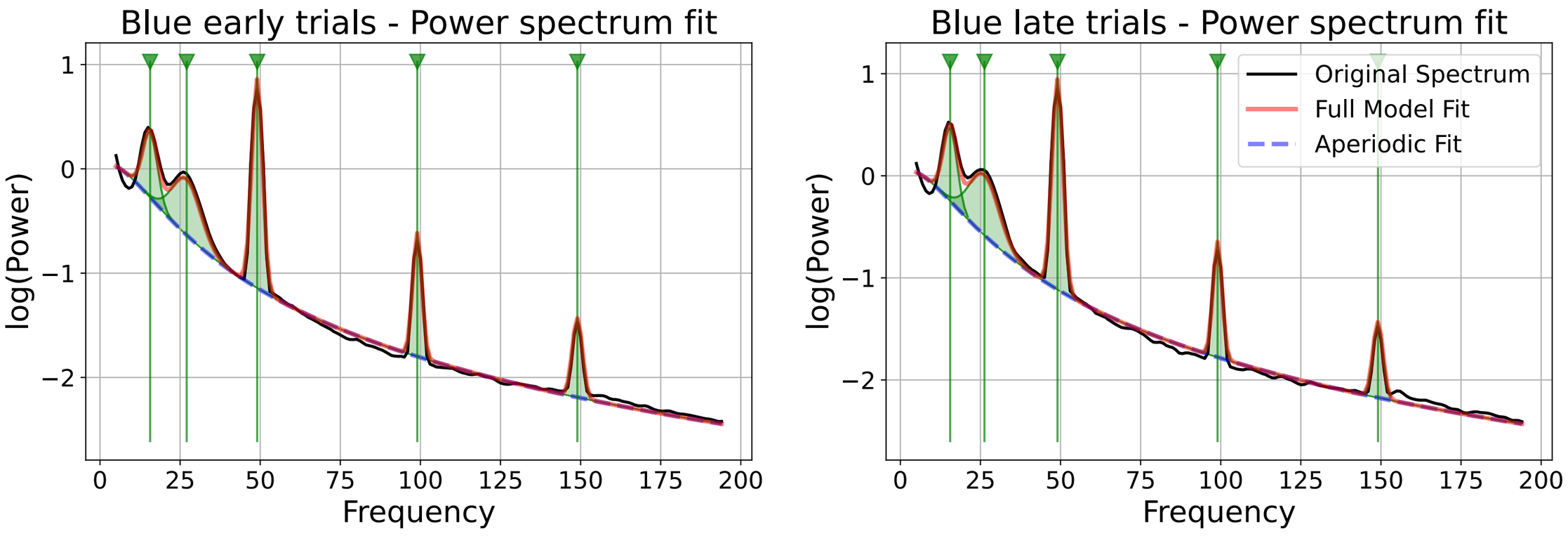

B

Monkey T

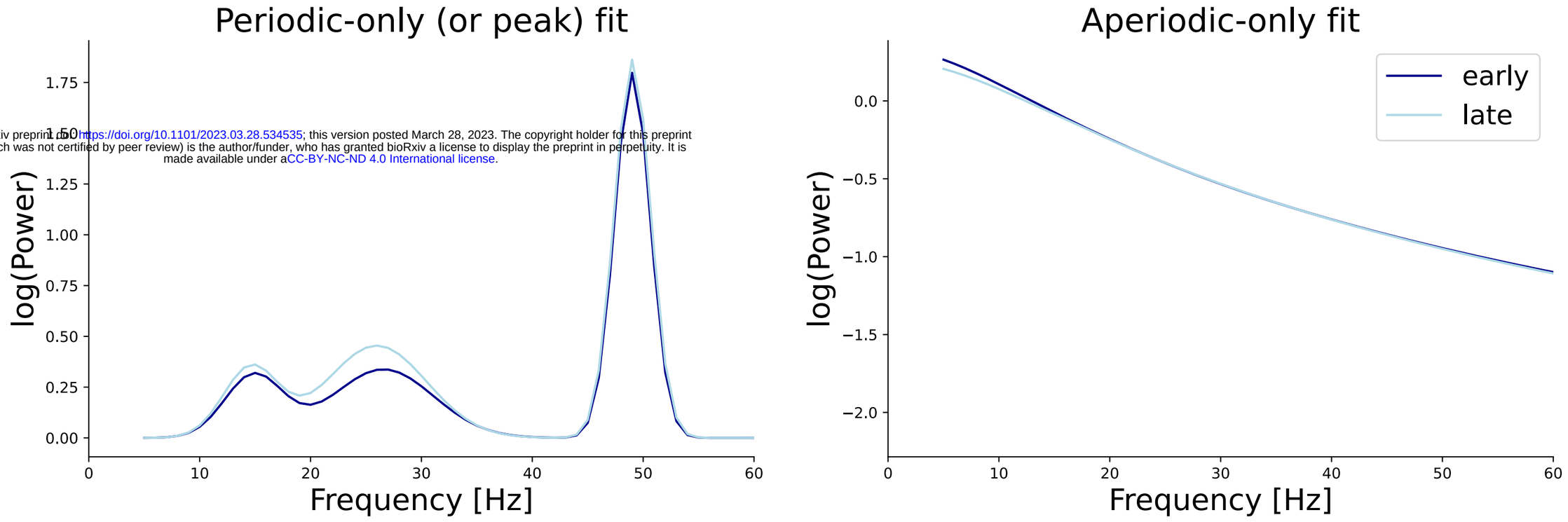

Monkey M

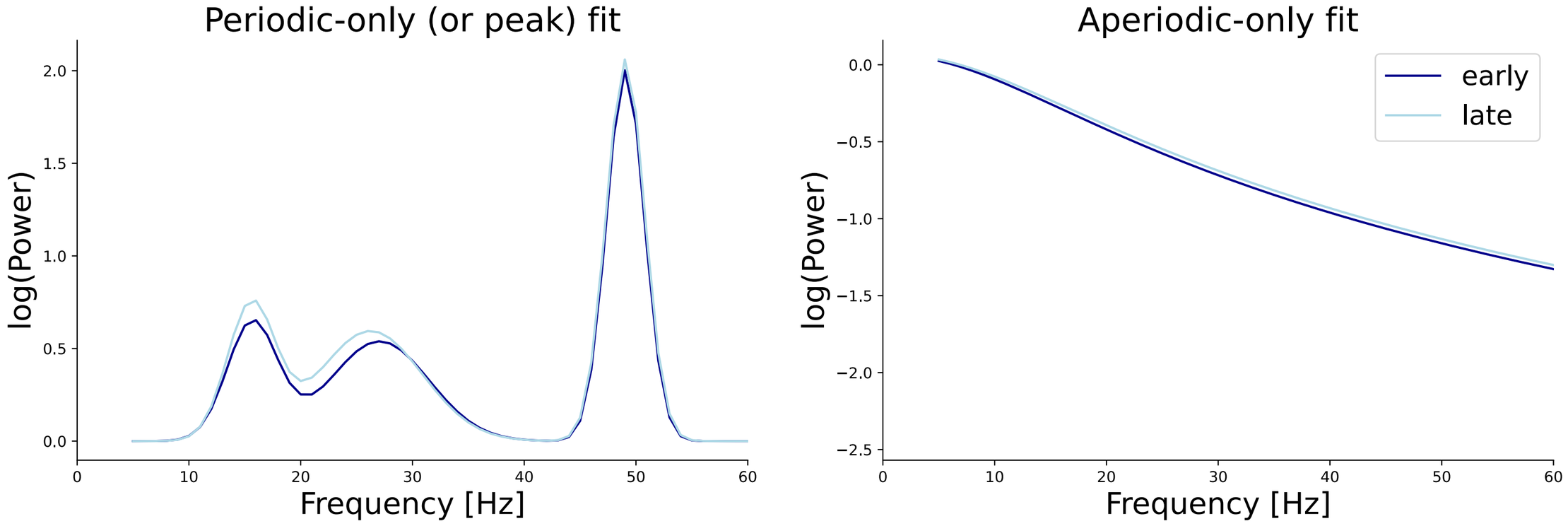

Suppl. Fig. 7. Spectral parametrization for early and late trials.

	Number of behavioral trials for each color condition and movement direction						
	Blue	**Green**	**Pink**	**UR**	**LR**	**LL**	**UL**
Monkey T	2261	1987	1766	1556	1647	1577	1234
Monkey M	2109	1821	1643	1396	1406	1383	1388
	Proportion of distractor errors (% of correct+distractor)						
	Blue	**Green**	**Pink**	**UR**	**LR**	**LL**	**UL**
Monkey T	20.7	20.4	16.7	19.4	16.8	18.6	23.7
Monkey M	30.8	27.3	11.2	27.1	23.5	23.9	24.2
	Reaction times in correct trials, from hand trajectories (ms)						
	Blue	**Green**	**Pink**	**UR**	**LR**	**LL**	**UL**
Monkey T	150 +/-40	152 +/-39	147 +/-50	150 +/-50	150 +/-38	147 +/ 37	152 +/-46
Monkey M	173 +/-57	169 +/-58	153 +/-65	170 +/-57	150 +/-62	163 +/-60	179 +/-59

Suppl. Table 1. Summary of number of trials included for behavioral analyses, percent of distractor errors and RTs for each color condition and movement direction for each animal. UR-upper right; LR-lower right; LL-lower left; UL-upper left.